Accepted Manuscript

A multifunctional therapeutic approach: Synthesis, biological evaluation, crystal structure and molecular docking of diversified 1H-pyrazolo[3,4-b]pyridine derivatives against Alzheimer's disease

Tarana Umar, Shruti Shalini, Md Kausar Raza, Siddharth Gusain, Jitendra Kumar, Prerna Seth, Manisha Tiwari, Nasimul Hoda

PII: S0223-5234(19)30353-8

DOI: https://doi.org/10.1016/j.ejmech.2019.04.038

Reference: EJMECH 11273

To appear in: *European Journal of Medicinal Chemistry*

Received Date: 5 March 2019

Revised Date: 3 April 2019

Accepted Date: 13 April 2019

Please cite this article as: T. Umar, S. Shalini, M.K. Raza, S. Gusain, J. Kumar, P. Seth, M. Tiwari, N. Hoda, A multifunctional therapeutic approach: Synthesis, biological evaluation, crystal structure and molecular docking of diversified 1H-pyrazolo[3,4-b]pyridine derivatives against Alzheimer's disease, *European Journal of Medicinal Chemistry* (2019), doi: https://doi.org/10.1016/j.ejmech.2019.04.038.

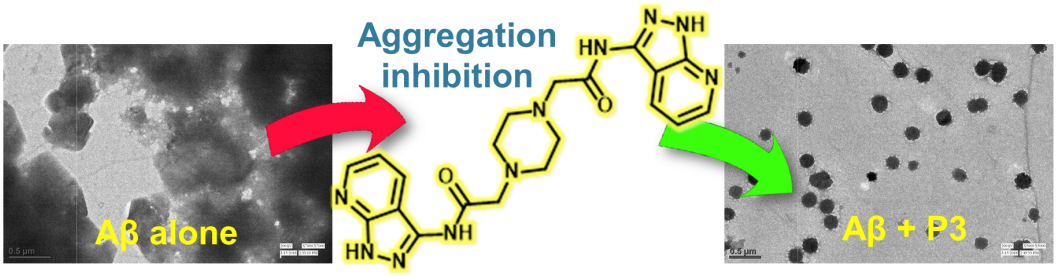

Inhibitors showed Aβ self-aggregation inhibition upto 81.65% and AChE inhibition upto IC_{50} 4.8 nM

A multifunctional therapeutic approach: Synthesis, biological evaluation, crystal structure and Molecular docking of diversified 1H-pyrazolo[3,4-b]pyridine derivatives against Alzheimer's disease

Tarana Umar [a], Shruti Shalini [‡b], Md Kausar Raza [‡c], Siddharth Gusain [b], Jitendra Kumar [d], Prerna Seth[b], Manisha Tiwari [b,*] and Nasimul Hoda [a,*]

[a] *Department of Chemistry, Jamia Millia Islamia (Central University), New Delhi 110025, India*
[b] *Dr. B. R. Ambedkar Centre for Biomedical Research, University of Delhi, New Delhi 110007, India*
[c] *Department of Inorganic and Physical Chemistry, Indian Institute of Science, Bangalore 560012, India*
[d] *Department of Chemistry, Sardar Vallabhbhai Patel College, Bhabua, Kaimur- 821101, V. K. S. U., Ara, Bihar- 802301, India*
‡These authors contributed equally to this manuscript.

Abstract

2-(piperazin-1-yl)-N-(1H-pyrazolo[3,4-b]pyridin-3-yl)acetamides are described as a new class of selective and potent acetylcholinesterase (AChE) inhibitors and amyloid β aggregation inhibitors. Formation of synthesized compounds (**P1-P9**) was justified *via* H^1 NMR, C^{13} NMR, mass spectra and single crystal X-Ray diffraction study. All compounds were evaluated for their acetylcholinesterase and butyrylcholinesterase inhibitory activity, inhibition of self-mediated Aβ aggregation and Cu(II)-mediated Aβ aggregation. Also, docking study carried out was in concordance with *in vitro* results. The most potent molecule amongst the derivatives exhibited excellent anti-AChE activity (IC_{50} = 4.8 nM). Kinetic study of **P3** suggested it to be a mixed type inhibitor. *In vitro* study revealed that all the compounds are capable of inhibiting self-induced β-amyloid (Aβ) aggregation with the highest inhibition percentage to be 81.65%. Potency of **P1** and **P3** to inhibit self-induced $A\beta_{1-42}$ aggregation was ascertained by TEM analysis. Compounds were also evaluated for their Aβ disaggregation, antioxidation, metal-chelation activity.

Keywords: N-(1H-pyrazolo[3,4-b]pyridin-3-yl)acetamides; AChE inhibitors; selectivity; amyloid β aggregation inhibitors; docking

* Corresponding author. Tel.: +0091-9910200655; fax: +0091-11-26985507; e-mail: nhoda@jmi.ac.in

* Corresponding author. Tel.: +0-000-000-0000; fax: +0-000-000-0000; e-mail: mtiwari07@gmail.com

1. Introduction

Alzheimer's disease (AD) is the devastating disease that strongly correlates to morbidity and mortality. AD is amongst the most predominant irreversible neurodegenerative disorders that targets to cholinergic neurons of central nervous system (CNS) together with cognitive ability and spatial awareness [1]. AD is recognized as the leading reason for dementia that mainly troubles old age groups, although cases of age groups belonging 30s, 40s and 50s had started to rise. The estimated figure of people suffering dementia in 2018 is 50 million worldwide and is in progression [2].

Etiology of Alzheimer's is not yet explained. However accumulation of amyloid beta [3], shortage of neurotransmitter acetylcholine [4], tau- phosphorylation and oxidative stress [5] are active participants in AD (pathophysiology) [6]. On account of its intricacy and as an answer to this pluralism of causative factors and consequences, one feasible research strategy is to evolve a multi targeted perspective, by which a unit molecule acts on separate targets of disease. Several attractive targets present good opportunity towards the development of anti-AD agents, and its multi-factorial nature demands multi-targeted molecules that may benefit AD treatment. It further allows to overcome intrinsic disputes of the combination therapy, where exists possibility of drug-drug interactions [7] and also to acquire superior therapeutic profile than single targeted molecules. Recognition of multifactor nature of AD is widespread. Simultaneous targeting of AD pathologies by exploiting independent and multiple activity drug therapies has come up as a very strong strategy to address the multiplex, degenerative character of AD. Where from the cholinergic and amyloid hypotheses are generally applied to originate reliable therapeutics.

The two capital modes have been described to be generously involved in disease growth: i) accumulation of the amyloid β in extracellular region in fibrils, protofibrils and plaques and ii)

continuous de-escalating of cholinergic neurons especially in cortex and hippocampus. Amassment of Aβ due to evacuation of Aβ and/or, changed processing of APP happens according to central AD hypothesis. The event leads to selective neuronal loss and widespread synaptic dysfunction.

Anomalous assembling of misfolded Aβ peptides depicts a crucial characteristic and is possibly the triggering mechanism for cognitive dysfunction in AD and neurodegeneration [8]. Amongst the various forms of Aβ derived from APP, the most abundant one is $A\beta_{1-42}$, having higher tendency to congregate into different oligomeric and fibrillar complexes [9]. $A\beta_{1-42}$ peptide is believed to primarily comprise the predominant portion of Aβ plaques in AD patients [10,11]. Over a period of time the increasing accumulation of these toxic aggregates markedly contributes towards downstream AD pathologies like oxidative damage, tangle formation, and neuronal apoptosis [12,13]. A number of studies have confirmed pathophysiological consequences of its neurotoxicity both by *in vitro* [14] and in vivo models [15].

On other part neurotransmitter acetylcholine (ACh) is critically important signaling molecule of cholinergic transmission [16]. Breakdown of this neurotransmitter befalls *via* the terminator enzyme of nerve impulse transmission, acetylcholinesterase at the cholinergic synapses. One protein that appears to fill a prominent place within the multiplex pathological network of this disease is AChE. It is a terminator enzyme of nerve impulse transmission at the cholinergic synapses. Degeneration of cholinergic system in AD accounts for the contribution towards cognitive impairment. This hypothesis asserts the declined ACh levels as it leads to cholinergic failure and hence cognitive impairment. AChE has exceptionally great specific catalytic activity, specifically for a serine hydrolase - each AChE molecule degrades approx. 25000 ACh molecules per second [17,18]. Crystal structure of *Torpedo californica* AChE (*Tc*AChE)

indicated presence of a 200nm long, narrow gorge on enzyme surface. Its bottom is referred to as catalytic active site, top as peripheral anionic site and there are five amino acid residues in middle. Acetylcholinesterase inhibitors function by interaction with the PAS, CAS or both. For molecule to actively bind to the gorge, it needs to have interacting groups at terminals that could possess CAS/PAS binding. In relation to this AChE inhibition may provide higher level of neurotransmitter in synaptic cleft, thereby upgrading cognition in mild-moderate level AD patients [19]. For a period AChEIs were known to bring about only symptomatic revival, lacking any influence on disease itself [20]. Nevertheless, other studies signify that AChE interacts with amyloid β *via* hydrophobic environment in vicinity of PAS, thereby promoting Aβ fibril formation [21,22]. Furthermore, the AChE-amyloid β complexes elevate the amyloid β dependent neurotoxicity [23]. These reports recreate interest in AChEIs. Several clinical trials revealed the e□cacy as well as safety of ChEIs in treating AD.

Oxidative stress is described amongst the early phenomena in AD pathogenesis [24]. Significance of oxidative damage in neuronal degeneration is also supported by the free radical and oxidative stress theory of aging. Hence, protection of neurons against oxidative damage could capably prevent AD. Recently molecules that modulate AChE inhibition, amyloid beta disaggregation and inflammation altogether have been seen to show successful results for AD [25]. With this frame of reference, the concept of multi-targeted agents exhibiting an integrated action on more than one neurobiological target associated with origination and development of the disease presently reassures the design of anti-Alzheimer's agents [26-28].

1H-Pyrazolo[3,4-b]pyridines are an eminent group of molecules owing to their variable biological as well as pharmacological action. They have been demonstrated to possess, among others, antimalarial [29], inhibition of cyclin-dependent kinases [30-35], GSK 3 inhibition [36],

antiproliferative [37], antileishmanial [37], cardiovascular [38,39] and antiviral [40-42] activities [43-45]. Investigation of molecules comprising 1H-Pyrazolo[3,4-b]pyridines has been developed owed to their diverse effects in miscellaneous domains [29,36,37]. The 4-amino-5-carboxylates of pyrazolo[3,4-b]pyridines; ethyl 1-ethyl-4-(2-(propan-2-ylidene)hydrazinyl)-1H-pyrazolo[3,4-b]pyridine-5-carboxylate (Etazolate) is an anxiolytic drug that has also been known for its neuroprotective nature [46]. A group of drugs from this scaffold; Tracazolate, Etazolate, LASSBio-872, LASSBio-873, LASSBio-981, and LASSBio-982 have been used to treat anxiety disorder related with GABA induced neuro-inhibition (Fig. 1).

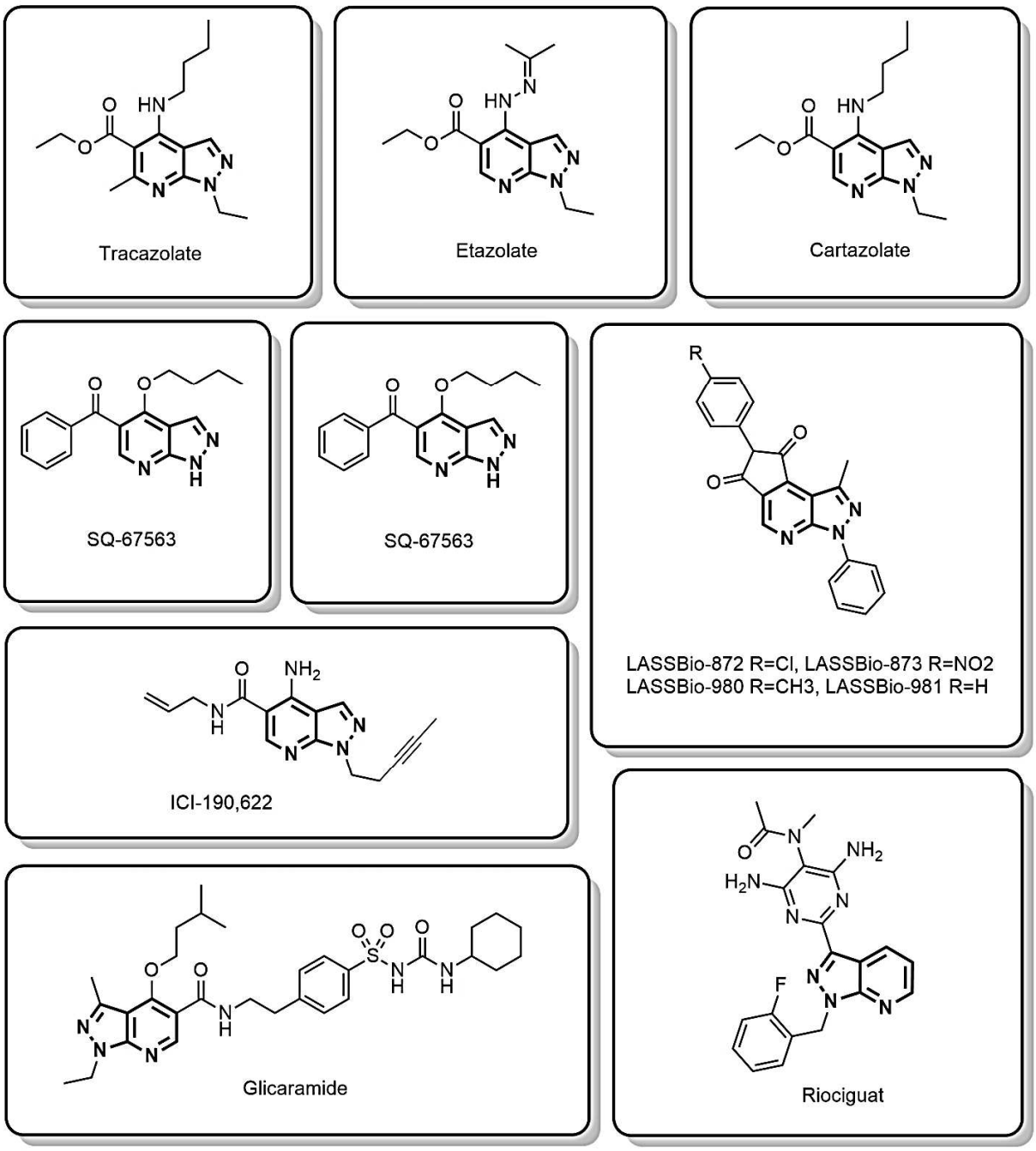

Fig. 1. Neurologically active drugs based on of pyrazolo[3,4-b]pyridines.

With present study we intend to develop potent neuroprotective agents against Alzheimer's disease derived from pyrazolopyridine and evaluate their biological activities. In this work we report the first synthesis of pyrazolopyridine acetamide derivatives of this kind as well as the X-

ray diffraction of two representative derivatives. In our preceding experimental project, a set of quinoline derivatives was synthesized as amyloid β aggregation inhibitors, antioxidants and metal chelators [47]. Thus, in the present study, further attempt has been made to search other potential scaffolds and compounds that possess multi-targeting potential. To explore more anti-Alzheimer's agents, we present here a diversified synthesis of 1H-pyrazolo[3,4-b]pyridine derivatives (**P1-P9**) as the new class in multi-functional Anti-Alzheimer's agents integrating anti-Aβ aggregation, AChE inhibition, radical scavenging and metal chelation activities in single molecule.

2. Results and discussion

2.1. Chemistry

The development of the diversified pyrazolopyridine derivatives (**P1-P9**) was accomplished *via* synthetic pathways shown in Scheme 1, 2 and 3. As a continuation of previous work [25] the previously synthesized intermediates 6(a,b) were used to synthesize new pyrazolopyridine compounds P1 and P2. Furthermore for some compounds we have tried to use the same combination of piperazine with quinoline in order to achieve better results. 1-{5-methyl-[1,2,4]triazolo[1,5-a]pyrimidin-7-yl}piperazine and ethyl 4-(piperazin-1-yl)quinoline-3-carboxylate derivative were prepared *via* three step method described previously [25] as given in Scheme 1 and 2. The 7-chloro-4-(piperazin-1-yl)quinolone [48] and 2-(piperazine-1-yl)pyridine-3-carbonitrile were prepared *via* nucleophilic aromatic substitution reaction (S_NAr) of piperazine on 4,7-dichloroquinoline and 2-chloro-3-cyanopyridine respectively. These piperazine derivatives and other piperazine analogues were reacted with the 2-chloro-N-(1H-pyrazolo[3,4-b]pyridin-3-yl)acetamide according to schemes 1, 2 and 3 to yield the final compounds **P1-P9**. The compounds were stable in solid states at RT. The ^{1}H NMR showed common signals around

13.33, 11.05, 8.51, 8.37 and 7.17 of the N-(1H-pyrazolo[3,4-b]pyridin-3-yl)acetamide fragment present in all the final compounds. The pyrazolopyridine NH was detected in a range of δ 13.34-13.25, as singlet peak for all inhibitors. The NHCO proton in all inhibitors occurred as singlet in range δ 10.81-10.26. The conversion of $COCH_2Cl$ to $COCH_2N$ shifted peak from more deshielded region δ 4.37 to less deshielded region below δ 4.00. Other aromatic and/or aliphatic substituents of compound were observed as expected. In a similar fashion common peaks for N-(1H-pyrazolo[3,4-b]pyridin-3-yl)acetamide fragment were observed in ^{13}C spectra. The peak for piperazine ring carbons was observed around 45 and 51 ppm. The different aromatic substituents showed their respective peaks.

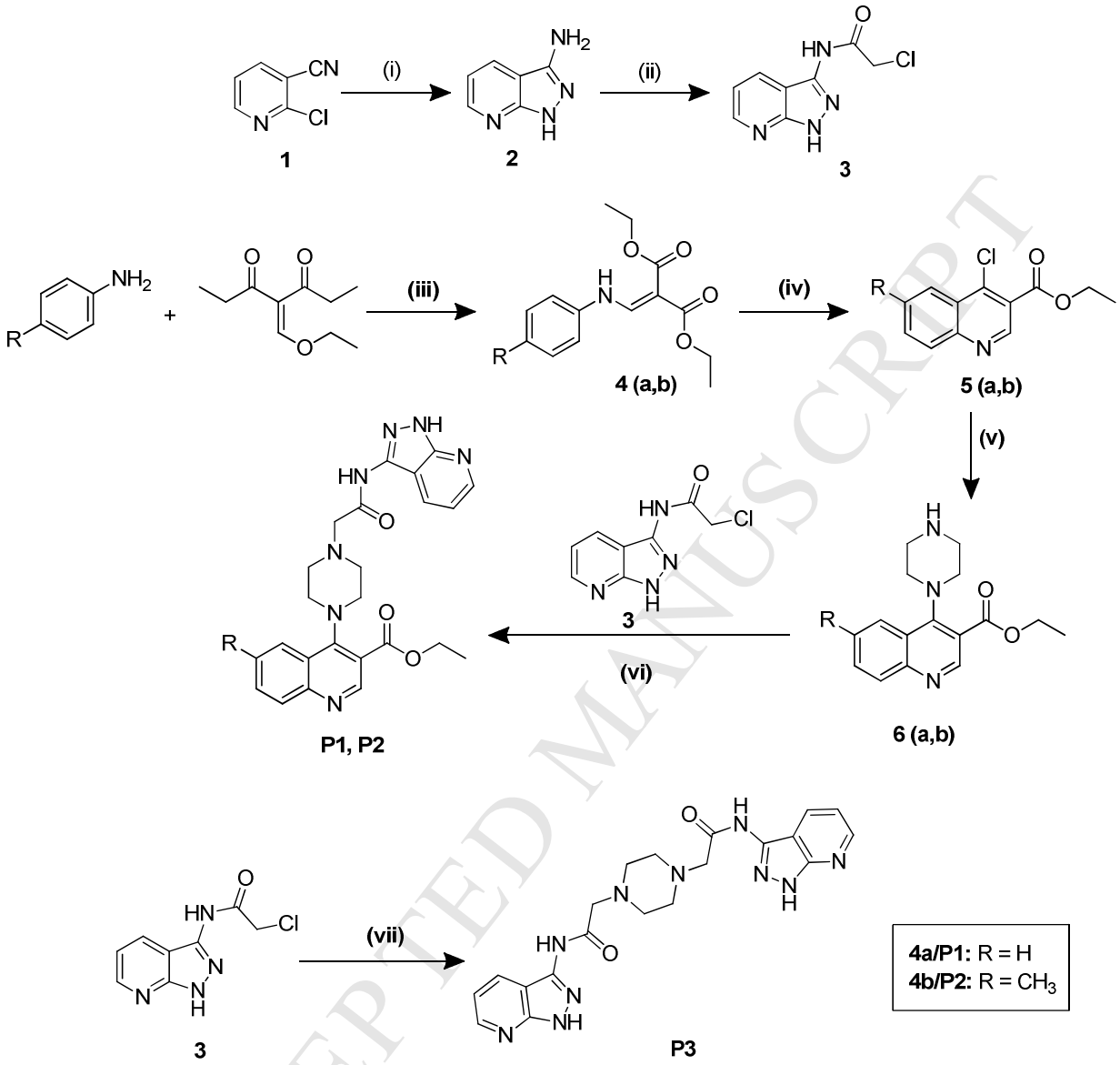

Scheme 1. Synthesis of 2-(4-substituted piperazin-1-yl)-N-(1H-pyrazolo[3,4-b]pyridin-3-yl)acetamide derivatives (**P1**, **P2**, **P3**). Reagents and conditions: (i) Hydrazine hydrate, EtOH, 60 °C; (ii) glac.AcOH, NaOAc, chloroacetyl chloride, RT; (iii) Benzene, 83 °C; (iv) $POCl_3$, 110 °C; (v) Piperazine, MeOH, reflux; (vi) TEA, THF, reflux; (vii) piperazine, TEA, THF, 60 °C.

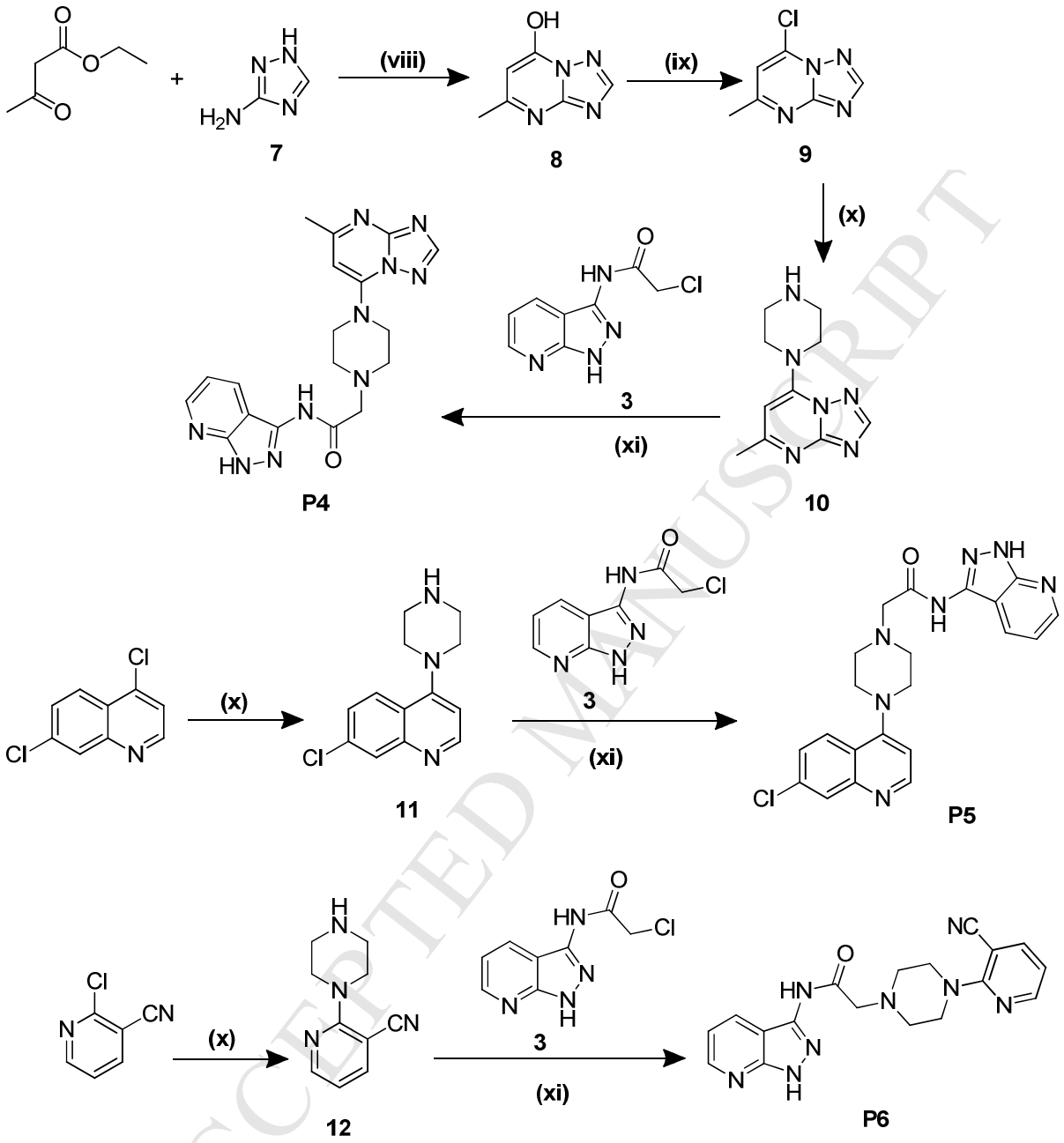

Scheme 2. Synthesis of 2-(4-substituted piperazin-1-yl)-N-(1H-pyrazolo[3,4-b]pyridin-3-yl)acetamide derivatives (**P4**, **P5**, **P6**) linked to 1-{5-methyl-[1,2,4]triazolo[1,5-a]pyrimidin-7-yl}piperazine (**10**), 7-chloro-4-(piperazin-1-yl)quinoline (**11**), and 2-(piperazine-1-yl)pyridine-3-carbonitrile (**12**) respectively. Reagents and conditions: (viii) Acetic acid, 110 °C; (ix) $POCl_3$, 110 °C; (x) piperazine, MeOH, reflux (xi) TEA, THF, reflux.

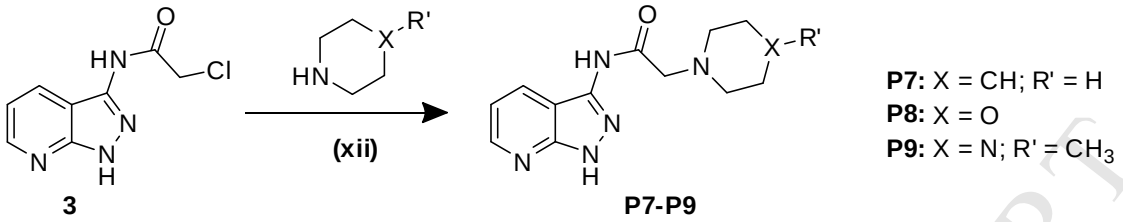

Scheme 3. Synthesis of 2-(4-substituted piperazin-1-yl)-N-(1H-pyrazolo[3,4-b]pyridin-3-yl)acetamide derivatives (**P7-P9**). Reagents and conditions: (xii) piperazine analogue, THF, 65 °C.

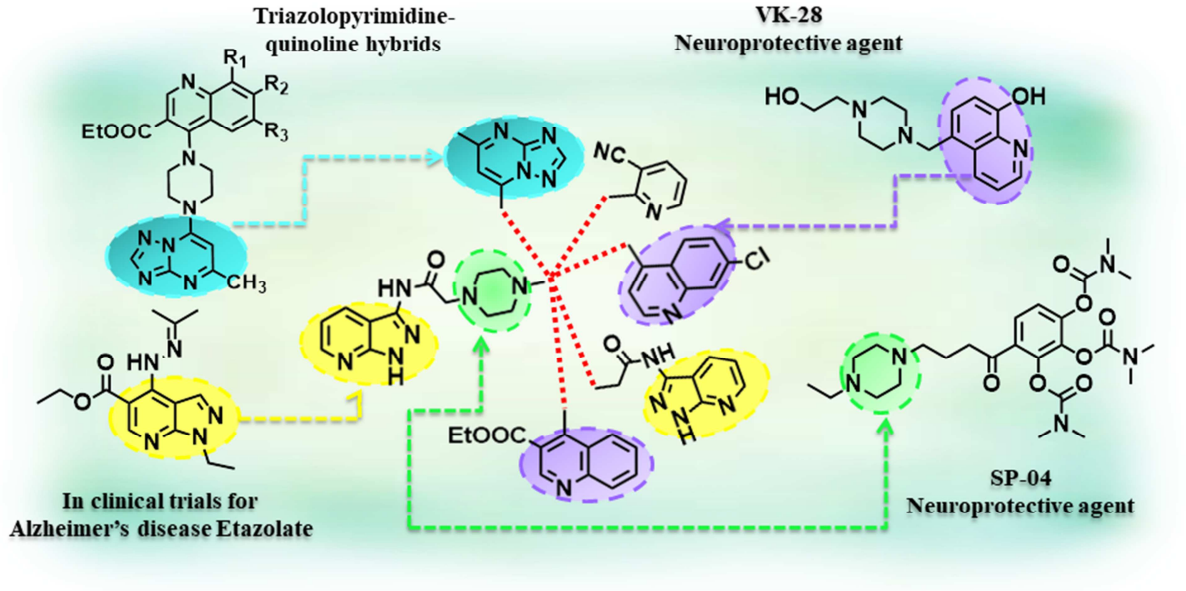

Fig. 2. Molecular strategy for pyrazolopyridine hybrid molecules; 2-(piperazin-1-yl)-N-(1H-pyrazolo[3,4-b]pyridin-3-yl)acetamide with triazolopyrimidine, pyrazolopyridine, quinoline and pyridine.

Aromatic residues cover the deep narrow gorge of the AChE active site. Thus using piperazine linker could increase molecule length and associate with π-cation interaction with aromatic gorge. Combination with scaffolds such as, pyrazolopyridine, quinoline, pyridine and

triazolopyrimidine was preferred choice having various valuable properties (see Fig. 2). Since pyrazolopyridine possesses a planar structure it is expected to favour intercalation between Aβ fibrils and inhibit aggregation. In AChE it is expected to engage with the CAS and PAS leading to preferred enzyme inhibition. Quinoline has a great biological background with neuroprotective effects, AChE inhibition, free radical scavenging and chelation. Quinoline was supposed to bind with CAS of AChE by π- π interaction as well as disaggregate Aβ sheets owing to its planarity. Incorporating various combinations of these scaffolds in one candidate as anti-Alzheimer's agent, we carried out a detailed *in vitro* study of these compounds on different hypothesis factors of AD.

2.2. Single crystal structure

X-ray crystallographic determination of **P6** and **P9** was carried out (Fig. 3, Table 1, and Fig. S29-S34, Supporting Information). **P6** crystallizes in P**121**/c**1** space group of monoclinic (Fig. 3a) and **P9** in P**212121** of the orthorhombic crystal system (CCDC number: 1870982 and 1870983) (Fig. 3b). The C-O bond distance of carbonyl group in both the compounds **P6** and **P9** was found to in between 1.2214(16) and 1.2155(19) Å respectively. The bond lengths of N(2)-N(3) in **P6** and **P9** were 1.3639(16) and 1.3599(17) Å, respectively. For compound **P6**, the N(2)-C(6), N(4)-C(6) and N(1)-C(1) bonds were of 1.3168(17), 1.4009(16) and 1.3260(20) Å whereas for compound **P9** it was 1.3134(18), 1.4098(17) and 1.334(20) Å, respectively. The bond angles between N(2)-C(6)-N(4) for both **P6** and **P9** were 116.48(11)º and 119.64(13)º whereas O(1)-C(7)-N(4) were 125.23(12)º and 123.70(13)º, respectively. The pi-pi stacking and H-bonding interactions along with short contact bonding for both the **P6** and **P9** compounds with their adjacent atoms were observed. The unit cell packing diagram of **P6** and **P9** was given in supporting information (Fig. S29-S34).

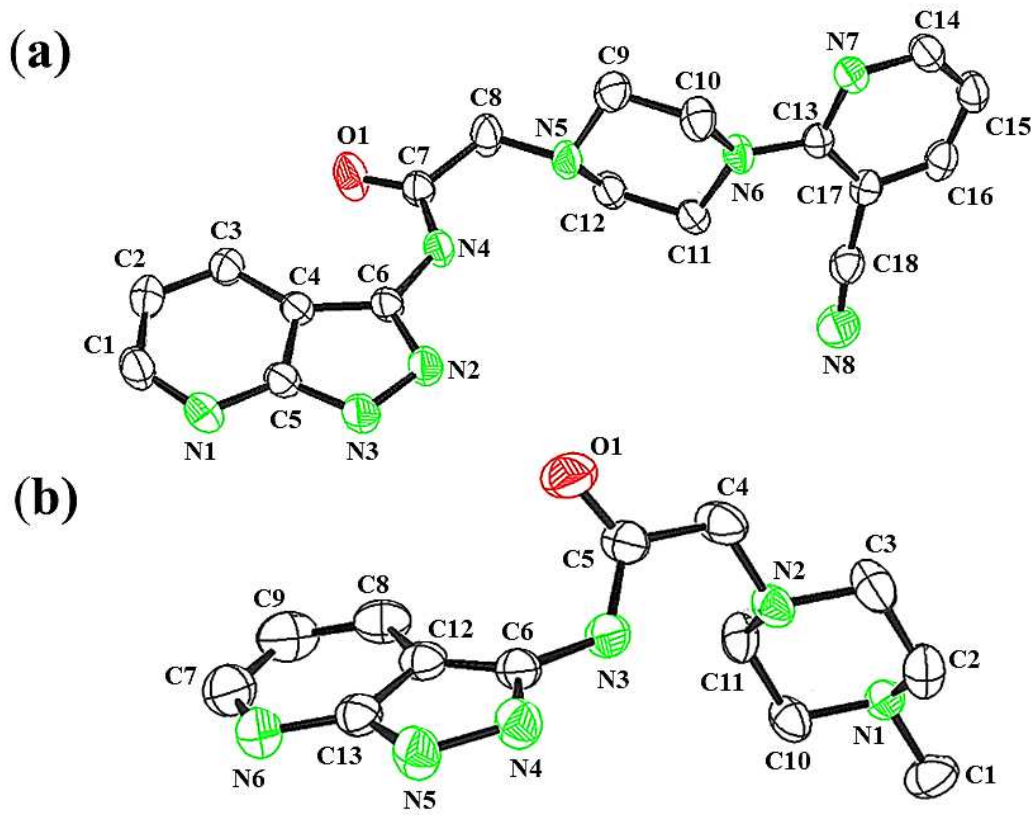

Fig. 3. ORTEP diagram of compounds **P6** (a) and **P9** (b) (50% probability level of thermal ellipsoids). Color codes: Carbon, black; Nitrogen, green and Oxygen, red. Hydrogen atoms are omitted for clarity.

Table 1. Crystal data and structure refinement for 2-(4-(3-cyanopyridin-2-yl)piperazin-1-yl)-N-(1H-pyrazolo[3,4-b]pyridin-3-yl)acetamide (**P6**) and (4-methylpiperazin-1-yl)-N-(1H-pyrazolo[3,4-b]pyridin-3-yl)acetamide (**P9**) respectively.

	P6	**P9**
Empirical formula	$C_{18}H_{18}N_8O_1$	$C_{13}H_{16}N_6O_1$
Formula weight	362.40	274.33
Crystal system	monoclinic	orthorhombic
Space group	P**121**/c**1**	P**212121**
a/Å	8.8090(10)	10.3642(6)

b/Å	26.311(3)	10.3714(6)
c/Å	7.8339(9)	13.0071(7)
α/°	90	90
β/°	110.743(3)	90
γ/°	90	90
V/Å^3	1698.0(3)	1398.15(14)
Z	4	4
T, K	273 (2)	273 (2)
ρ_{calcd}/g cm^{-3}	1.4175	1.303
λ/Å (Mo-Kα)	0.71073	0.71073
Data/restraints/param	3920/0/244	3234/0/183
F(000)	760	584
GOF	1.0566	1.110
$R(F_o)$,[a] I > 2 σ(I) [$wR(F_o)$[b]]	0.0430 [0.1082]	0.0345 [0.1019]
R (all data) [wR (all data)]	0.0503 [0.1138]	0.0370 [0.1037]
Largest diff peak, hole (e Å^{-3})	0.2864, -0.2429	0.178, -0.157
w = 1/[$(\sigma F_o)^2$ + $(AP)^2$ + (BP)]	A = 0.0547, B = 0.5255	A = 0.0592, B = 0.1561

[a] $R = \Sigma|F_o| - |F_c|/\Sigma|F_o|$. [b] $wR = \{\Sigma[w(F_o^2 - F_c^2)^2]/\Sigma[w(F_o)^2]\}^{1/2}$; where $P = (F_o^2+2F_c^2)/3$

Table 2. Selected bond distance (Å) and bond angle (°) for complex **P6** and **P9** with estimated standard deviations in parentheses.

	P6	**P9**
O(1)-C(7)	1.2214(16)	1.2155(19)
N(4)-C(7)	1.3376(16)	1.3439(19)
N(4)-C(6)	1.4009(16)	1.4098(17)
N(2)-C(6)	1.3168(17)	1.3134(18)
N(3)-C(5)	1.3468(17)	1.3524(19)
N(1)-C(1)	1.3260(20)	1.334(20)

N(4)-C(5)	1.3455(17)	1.4046(19)
N(2)-N(3)	1.3639(16)	1.3599(17)
N(8)-C(18)	1.145(2)	-
N(8)-C(18)-C(17)	174.18(16)	-
O(1)-C(7)-N(4)	125.23(12)	123.70(13)
O(1)-C(7)-C(8)	119.95(12)	120.58(14)
N(2)-C(6)-N(4)	116.48(11)	119.64(13)
N(3)-C(5)-N(1)	125.53(12)	111.20(11)
C(1)-N(1)-C(5)	113.50(12)	112.96(15)

2.3. Molecular docking studies

2.3.1. Molecular docking of P1, P2 and P3 with amyloid β

Neurotoxicity of amyloid peptide is connected to Aβ fibril generation. Development of a β-sheet pattern may assist aggregation of $A\beta_{1\text{-}42.}$ Hence, entities which hold the capacity to restrain β-sheet formation were helpful in Aβ aggregation inhibition. The action of β-sheet conformational change during fibrillogenesis is majorly stabilized by a Asp23/Glu22 and Lys28 residue salt bridge in $A\beta_{1–42}$ [49] and hydrophobic interactions. To elaborate the possible binding modes of inhibitors with Aβ, **P1**, **P2** and **P3** were chosen for computational study with the help of Auto Dock software and PyMOL to develop the images. PDB:1IYT was selected for the docking. From Fig. 4, all of these three compounds are situated near the vicinity of Aβ C-terminus and majorly stabilized through the hydrophobic bonding with His13, Lys16, Leu17, Ala21, Phe20, Glu22, Asp23, Val24, Lys28, Gly29, Ile31, Ile32, Leu34 and Met35 residues. In both Fig. 4 (a) and 4 (b), a strong intermolecular H-bonding existed between oxygen of carbonyl of carboxylate and hydrogen of N-H of Lys16 with

average distance of 1.8 Å. An intramolecular H-bonding existed between hydrogen of amide of N-H and oxygen of carbonyl of carboxylate at a closest distance of 2.3 Å and 2.8 Å respectively. In addition, three strong H-bondings existed between the hydrogen of N-H of amide and oxygen of hydroxyl of Glu22 (Fig. 4 (c)), another hydrogen of N-H of amide and oxygen of carbonyl of carboxylic acid, and hydrogen of N-H of pyrazolo ring and oxygen of hydroxyl of carboxyl group of Asp23 (average distance 2.1 Å, 2.3 Å and 2.6 Å respectively). Upon analyzing the outcomes of molecular modeling, we propose that inhibitors **P1**, **P2** and **P3** bind strongly with $A\beta_{1\text{-}42}$ and potentially interfere with β-sheets formation and inhibit Aβ aggregation. Molecular docking studies showed these test inhibitors to effectively bind with Aβ, inhibit the toxic conformation of $A\beta_{1\text{–}42}$ and stabilize the α-helical content. Inhibition assays revealed a lead compound with tight binding in the nanomolar range.

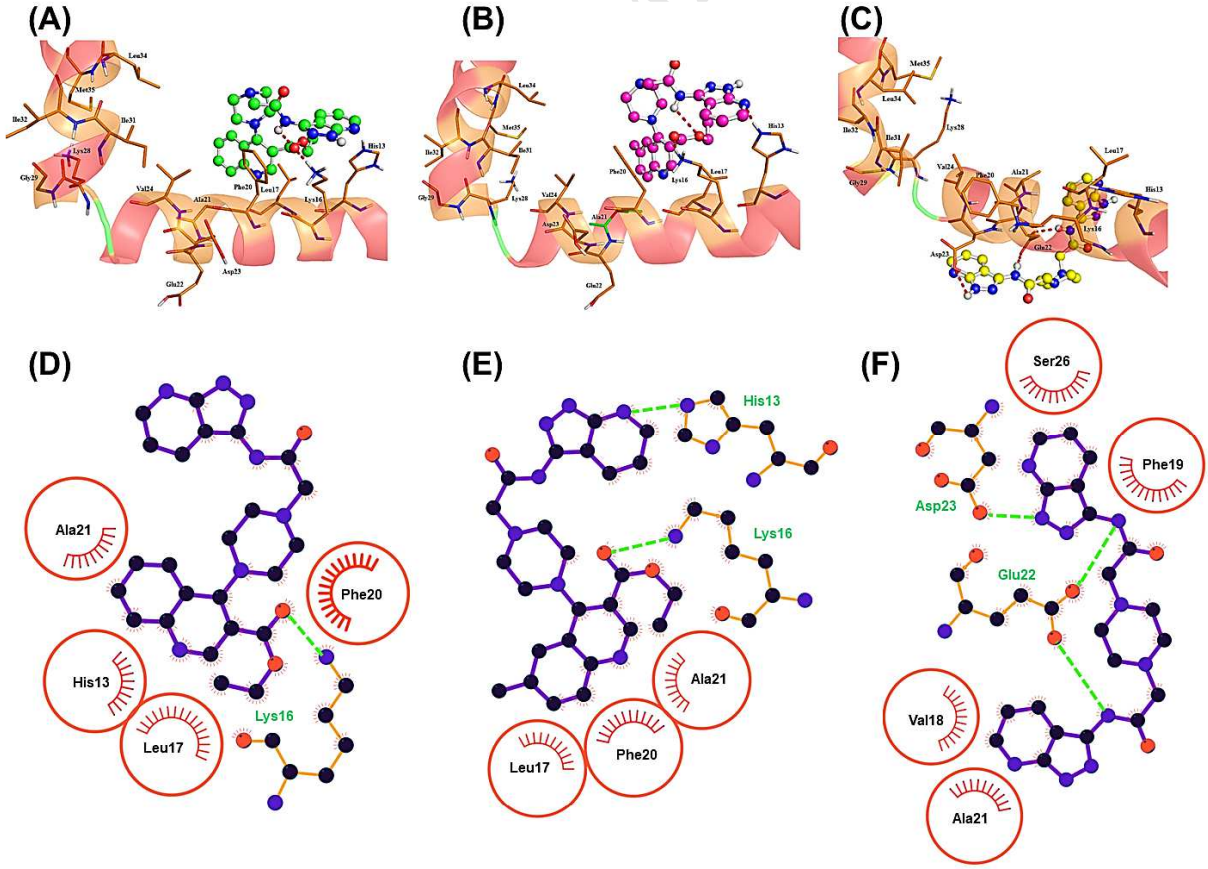

Fig. 4(a). Association of **P1** (oxygen as red, nitrogen coloured blue and carbon coloured green) and $A\beta_{1-42}$ C-terminus *via* molecular docking; **(b)** Association of **P2 (**oxygen as red, nitrogen coloured blue and carbon coloured magenta) and $A\beta_{1-42}$ C-terminus *via* docking calculations; **(c)** Association of **P3** (oxygen as red, nitrogen coloured blue and carbon coloured yellow) and $A\beta_{1-42}$ C-terminus *via* molecular docking. The H-bonding interactions are indicated with red dashed lines. Plot (D, E, F) represents the 2D view of docking interactions for inhibitors (**P1**, **P2**, **P3**) respectively by Ligplot. Green dashed line represents the H-bonds.

2.3.2. Free energy calculation by molecular docking of inhibitors with AChE

Synthesized inhibitors were docked with AChE (PDB Code 1EVE) in the active site. The positive control taken here for this computational study was Donepezil, displaying similar interactions as given in literature. Position of compounds **P3** corresponding to the binding site key residues is given in Fig. 5. Each of the two pyrazolopyridine moieties present in compound **P3** are involved in π-π stacking with Trp84 and Trp279 at distance of 3.3 Å and 5.1 Å respectively. In addition, there are three intermolecular hydrogen bonding. Firstly, an intermolecular hydrogen bonding is observed between carbonyl group of carboxyl of Asp72 with hydrogen of N-H of 1H- Pyrazolo[3,4]pyridine at average distance of 2.3 Å. Another two intermolecular hydrogen bondings are shown among oxygen of carbonyl group of amide bond with hydrogen of hydroxyl of Tyr121 and carbonyl group of Asp285 with hydrogen of N-H of 1H- Pyrazolo[3,4]pyridine having average distance of 2.4 Å and 1.7 Å respectively. The high binding affinity indicates that the selected inhibitors possess dual binding affinity owing to π-π stacking, hydrophobic binding and H-bonding.

Table 2. The free energy values of P1-P9 intermolecular docking using ParDOCK

Inhibitors	**Calculated free energy (Kcal/mol)**

	AChE (PDB ID: 1EVE)
P1	-7.81
P2	-9.11
P3	-9.32
P4	-5.58
P5	-7.41
P6	-7.47
P7	-4.31
P8	-4.18
P9	-4.58
Donepezil	-6.96
Tacrine	-4.90

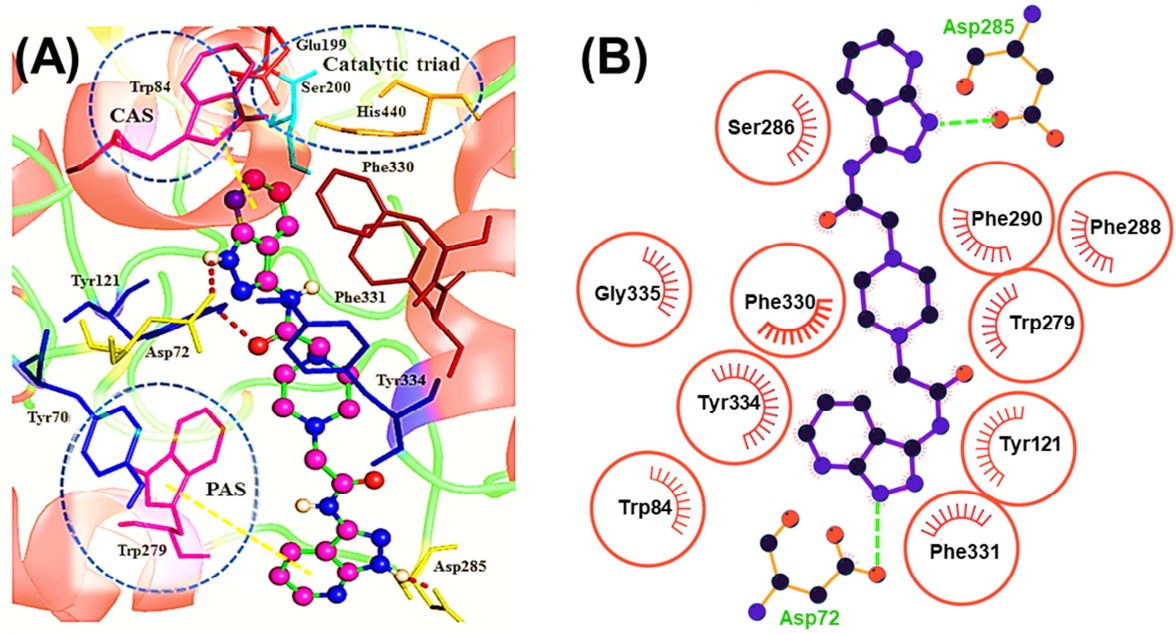

Fig. 5. The inhibitor is shown in ball and stick model while the key residues are shown in stick model. Different residues are represented by individual colors like Glu199 (red), Ser200 (Cyan), and His440 (Orange), Phe330, Phe331 (firebrick), Tyr70, Tyr121, Tyr334 (Blue), Trp84, Trp279 (Hot-pink), Asp72, Asp284 (Yellow). Other residues are shown in stick representation with

carbons coloured pink. Oxygen and nitrogen atoms in the complexes are coloured red and blue respectively. Plot **(A)** depicts interaction of **P3** with active site key residue of AChE and plot **(B)** Ligplot representation. π-π stacking is displayed as yellow dashed lines and intermolecular hydrogen bonding are shown by red broken lines. Hydrogen atoms removed for clarity. Structure is drawn through PyMol.

2.4. Pharmacological evaluation

2.4.1. Cholinesterase inhibitory activity (AChE and BuChE)

The inhibition potencies of the target inhibitors against both cholinesterase enzymes were evaluated *via* Ellman's method having Donepezil used as the reference molecule. Here, the AChE enzyme hydrolyses acetylthiocholine giving acetate and thiocholine. The thiocholine thus produced reduces the Dithiobis-Nitrobenzoic acid producing nitrobenzoate that absorbs at 412 nm. In a similar fashion, BuChE hydrolyses butyrylthiocholine giving butyrate and thiocholine. The potency and selectivity of the nine test inhibitors are summarized in Table 2. Most of the synthesized inhibitors showed very good inhibition potential in comparison to Donepezil (49 nM) with IC_{50} ranging from 4.8 nM to 113 nM. Compound **P7** displayed the maximum inhibition of AChE with IC_{50} of 4.8 nM followed by compound **P9** with an IC_{50} of 4.9 nM. However no significant inhibition of BuChE was observed by the compounds up to 100 μM concentration, suggesting the extremely selective nature of the test compounds towards AChE. The results of compound **P7**, **P8**, and **P9** suggest that the N-(pyrazolo[3,4-b]pyridinyl)acetamide clubbed with piperazine analogues possesses satisfactory inhibitory potential. The results of other compounds suggest that the inhibitory action of synthesized molecules was highly influenced with substitutions in N-(pyrazolo[3,4-b]pyridinyl)acetamide. SAR studies of the compounds revealed that the cholinesterase inhibition is minimal for compounds having an

adjacent electron withdrawing substituent at the deactivated aryl ring as in compounds **P1, P2** and **P6** (IC_{50} (AChE) >100 μM). Most likely the ester substituent on the quinoline ring and cyano substituent on pyridine ring laid their lower inhibitory activity. On comparing **P1** and **P2** with analogous compound **10a** [25,] we observe a decrease in cholinesterase activity. Reasonably good activity was found for compounds with sterically favorable and active side groups like **P3**, **P4** and **P5**. Maximal activity was found for the compounds with small molecules as substituents on the piperazine ring (compound **P9**). However, presence of morpholine ring in compound **P8** contributed to quite lower inhibitory activity than **P9**.

Table 3. Table for AChE and BuChE inhibition by synthesized inhibitors and the selectivity index for AChE.

Compounds	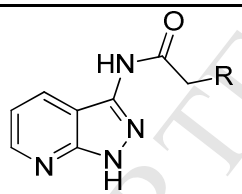 **(R=)**	**IC_{50} ± SD(μM)** **AChE[a]**	**BuChE[b]**	**Selectivity[c]** **BuChE/AChE**
P1	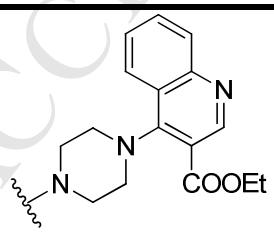	>100	>100	-

P2	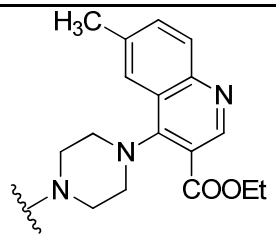	>100	>100	-
P3	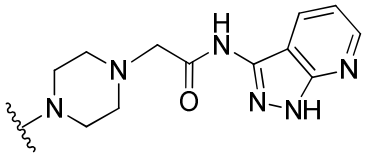	0.045 ±0.010	>100	>2222.22
P4	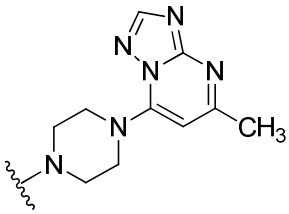	0.022 ±0.009	>100	>4545.45
P5	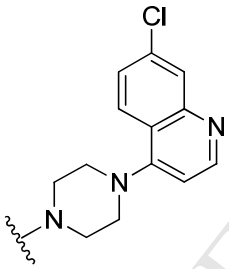	0.012 ±0.006	>100	>8333.33
P6	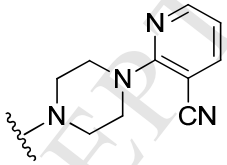	>100	>100	-
P7	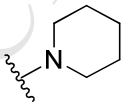	0.0048 ±0.001	>100	>20833.33
P8	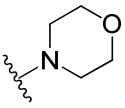	0.113 ±0.052	>100	>884.955

P9	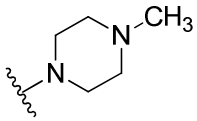	0.0049 ±0.001	>100	>20408.163
Donepezil	-	0.049 ± 0.05	8.71 ± 1.36	166.7

[a]AChE; inhibitor concentration (mean ± SD for these experiments) corresponding to 50% inhibition of AChE.

[b]BuChE; inhibitor concentration (mean ± SD for these experiments) corresponding to 50% inhibition of BuChE.

[c]Selectivity for AChE: $IC_{50\ (BuChE)}/IC_{50\ (AChE)}$.

2.4.2. Kinetic study of AChE inhibition

Study for mechanism was carried out with the active multifunctional compound **P3**. A Lineweaver–Burk double reciprocal plot was generated and is shown in Fig. 6. The graphical analysis shows the interception of lines in the plot above the x-axis with rise in slope (decreased Vmax) and increase in intercepts (higher Km) at elevating concentrations of compound. This indicates a mixed-type inhibition, verifying that **P3** might interact with both the CAS and PAS of AChE.

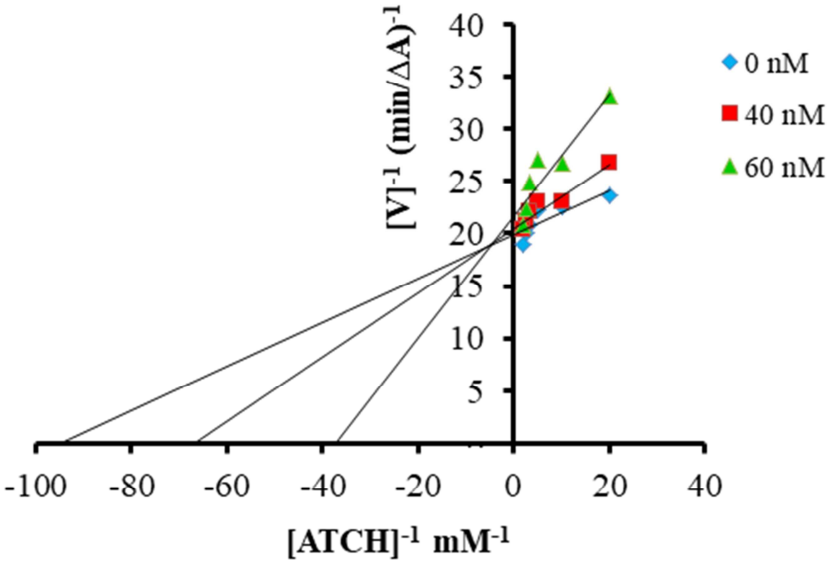

Fig. 6. Kinetic study of AChE inhibition mechanism with compound **P3**. Lineweaver–Burk reciprocal plot of AChE initial velocity with increasing substrate concentrations.

2.4.3. Self-mediated $A\beta_{1-42}$ aggregation inhibition study

A significant pathological characteristic linked with AD is amyloid plaques. Amyloid assembly initiates from disordered amyloidogenic protein monomers that are incorporated into a cascade of protein interactions to form a critical nucleus which later commences to adopt a cross β sheet of amyloid [50]. Aβ is produced *via* enzymatic cleavage of amyloid precursor protein which is usually present in the synapses of neuronal cells by α-, β-, and γ-secretases. The $A\beta_{40}$, variant of length 40 residues is the most prevalent form however, the 42-residue variant is more hydrophobic and aggregation prone. This $A\beta_{42}$ is the predominant one in the amyloid plaques.

Targeted compounds were tested for their $A\beta_{1-42}$ aggregation inhibition potential *via* the ThT fluorescence method. ThT is a fluorophore which displays an elevation in fluorescence on binding to amyloid fibrils.

Most inhibitors displayed a very good inhibition ranging from 50.60% to 81.64% in comparison to curcumin's 52.70 %. Compounds **P4**, **P5** and **P6** showed lower inhibition against amyloid

aggregates. This may be due to the presence of aromatic rings that provides rigidity, reduced flexibility and less favourable structures to intercalate between the amyloid fibrils. However the data for compounds **P1**, **P2**, **P3** and **P8** exhibiting aggregation inhibition of 81.65%, 69.31%, 79.47% and 74.62% respectively, suggests that both the presence of a sterically favourable structure and a substitution having interactive sites is important. On comparing compounds **P1** and **P2** with analogous compound **10a** [25] we observe an increase in inhibition percentage which is probably due to increase in interactive groups which bind with fibrils to disturb the aggregation. Most of our compounds showed higher inhibition with respect to the standard curcumin. Presence of a diamide linker on both head and tail regions in **P3** increased polarity and provided flexibility similar to Curcumin and contributed towards its activity. Increased hydrophobicity in tail region of compounds **P1** and **P2** resulted in their high inhibitory potency.

Table 4. Percent inhibition of $A\beta_{1-42}$ aggregation, percent disaggregation and ORAC trolox equivalents of synthesized inhibitors.

Compounds	**Self $A\beta_{1-42}$ aggregation inhibition[a] (%)**	**$A\beta_{1-42}$ disaggregation[b] (%)**	**Trolox equiv[c]**
P1	**81.646 ±3.06**	**61.59 ±2.16**	0.274 ± 0.08
P2	**69.306 ±1.84**	52.13 ±1.24	0.271 ± 0.06
P3	**79.472 ±2.65**	**53.80 ±1.82**	0.283 ± 0.07
P5	23.600 ±0.32	nd[d]	0.216 ± 0.07
P4	43.433 ±0.41	nd[d]	0.286 ± 0.10
P6	39.976 ±0.27	nd[d]	0.163 ± 0.08
P7	50.607 ±0.78	nd[d]	**0.650 ± 0.10**
P8	**74.619 ±2.54**	47.36 ±1.62	0.192 ± 0.06

P9	50.848 ±0.83	nd[d]	**0.362 ± 0.17**
Curcumin	52.70 ± 1.67	-	n.d
Resveratrol[e]	-	61.0	-

[a]The Th-T fluorescence assay was employed. Percent inhibition of aggregation (means ± SD) taken at inhibitor concentration of 25 μM.

[c]Percent disaggregation of $A\beta_{1-42}$ (mean± S.D) exhibited by compounds

[c]Data are expressed as μM of trolox equivalent/μM of tested compound (mean ± SD of three experiments).

[d]nd, not determined.

[e]taken from reference of Chuanjun Lu et al. [51]

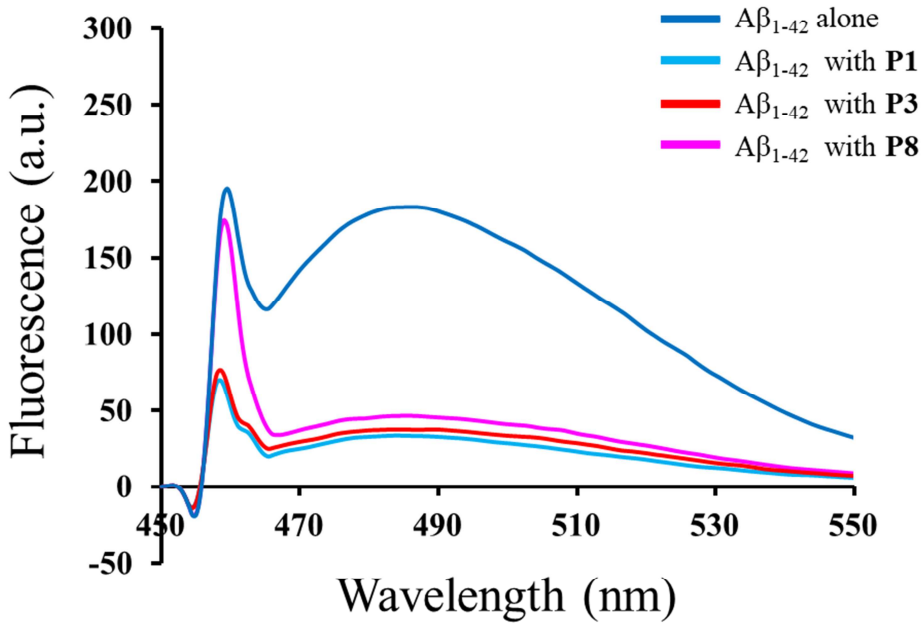

Fig. 7. Fluorescence intensity of $A\beta_{1-42}$ alone (dark blue), $A\beta_{1-42}$ with **P1** (light blue), $A\beta_{1-42}$ with **P3** (red), $A\beta_{1-42}$ with **P8** (pink) measured using ThT assay.

2.4.4. Disaggregation study of self-mediated Aβ Aggregation

The Amyloid plaques result from increase in $A\beta_{1-42}$ peptide production and accumulation. This $A\beta_{1-42}$ peptide oligomerizes and gets deposits as senile plaques. The compounds possessing a higher potential to inhibit self-induced Aβ aggregation were tested for their disaggregation potential against self-mediated $A\beta_{1-42}$ aggregation fibrils using a ThT assay. Compounds **P1**, **P2**, **P3** and **P8** were taken based on their high potency to inhibit self-mediated Aβ aggregation. Fresh Aβ was incubated for 48 h at 37° to enable the formation of fibrils. Then selected inhibitor was added to the sample and incubated for additional 24 h. Disaggregation of Aβ was measured *via* ThT assay, where the fluorescence intensity indicates degree of Aβ fibrillar aggregation. ThT stains amyloid deposits. **Table 4** demonstrates the $A\beta_{1-42}$ disaggregation inhibition (%) of the compounds and all four compounds exhibited a considerably high disaggregation percent. Compound **P1** and **P3** revealed the most favorable disaggregation results with 61.43% and 53.63% respectively, followed by **P2** with 51.95% and **P8** with 47.17%. High disaggregation by **P1** and **P3** is in concordance with the inhibition of self-induced Aβ fibril aggregation results.

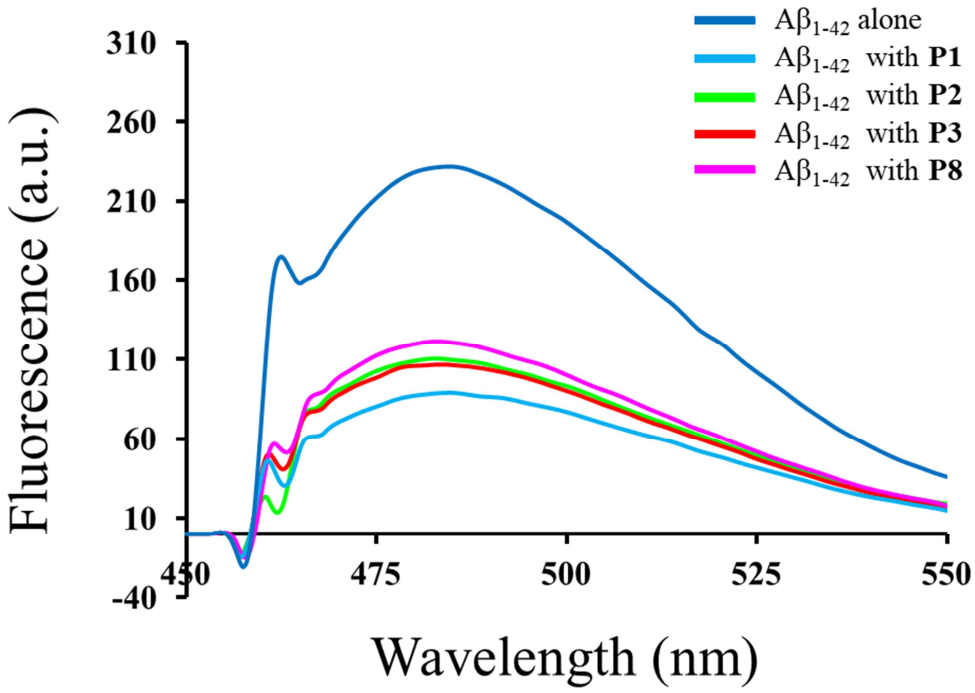

Fig. 8. Fluorescence intensity of $A\beta_{1-42}$ alone (dark blue), $A\beta_{1-42}$ with **P1** (light blue), $A\beta_{1-42}$ with **P2** (green), $A\beta_{1-42}$ with **P3** (red), $A\beta_{1-42}$ with **P8** (pink) measured using ThT assay.

2.4.5. Concentration dependent self Aβ aggregation inhibition study

Table 5. Percent inhibition of self- mediated Aβ aggregation by different concentrations of drug

Inhibitors	**$A\beta_{1-42}$ aggregation inhibition (%) [a]**				
	10μM	**15μM**	**20μM**	**25μM**	**IC_{50}**
P1	28.62	43.79	84.10	81.64	15.72μM
P3	3.9	39.85	58.04	79.4	17.89μM

[a] % inhibition of self-mediated Aβ aggregation (mean ± S.D) after incubation of 25 μM $A\beta_{1-42}$ with 10, 15, 20 and 25 μM compounds as indicated.

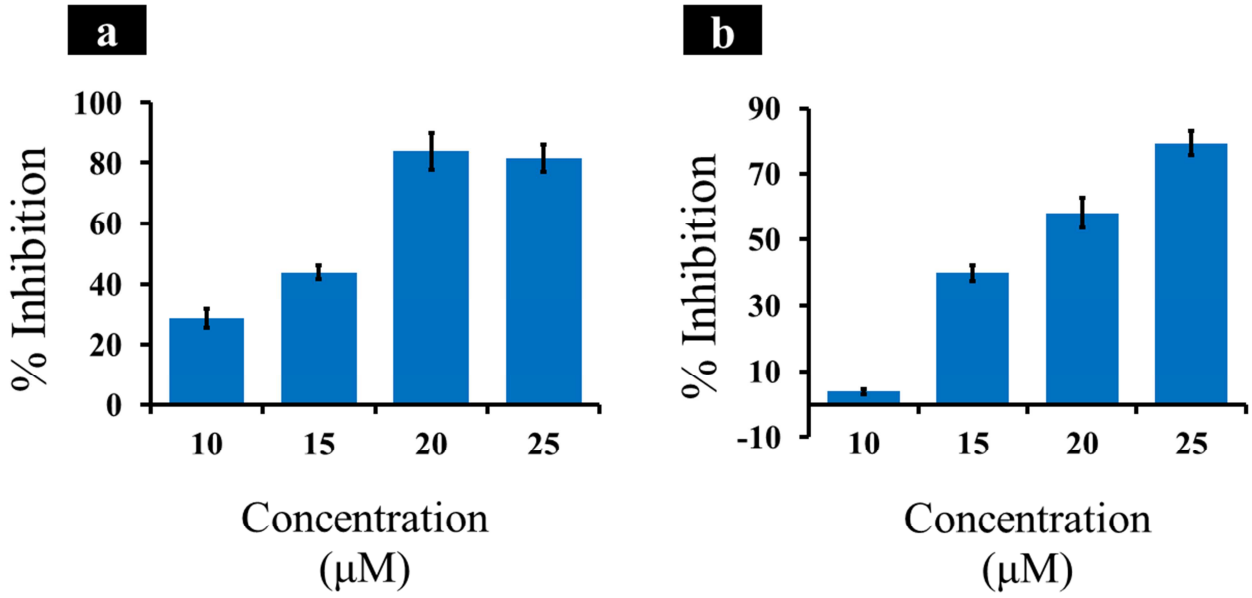

Fig. 9. Percent inhibition of self-mediated Aβ aggregation at four concentrations of drug (10, 15, 20 and 25 μM). The bar graph depicts a proportional relation between increase in concentration and % inhibition for compounds **P1** (a) and **P3** (b).

Concentration dependent self Aβ aggregation inhibition study was carried out in order to find the concentration-Aβ aggregation inhibition pattern. Compounds having the highest self Aβ aggregation inhibition and Aβ disaggregation were tested in this study. Inhibition of compounds **P1** and **P3** towards Aβ aggregation was observed at four different concentrations 10 μM, 15 μM, 20 μM and 25 μM. Sample of each concentration were incubated with fresh $A\beta_{1-42}$ for 48 h at 37 °C, and inhibition was measured using ThT fluorescence assay. A general trend of increase in Aβ aggregation inhibition with increase in concentration was observed for compound **P3**, whereas compound **P1** showed the highest inhibition at 20 μM. Compound **P1** exhibits high inhibition percentage at both 20 μM (84.10%) and 25 μM (81.64%). Altogether the results indicated a high inhibition for both compounds at 25 μM. Table 5 summarizes the inhibitory activity of both

compounds towards Aβ aggregation at different concentrations. The IC_{50} values calculated from the above result were 15.72 µM for compound **P1** and 17.89 µM for **P3**.

2.4.6. Aβ fibril formation inhibition study monitored through TEM

Confirmation of the higher inhibition potency exhibited by **P1** and **P3** were performed by a TEM analysis. As seen in TEM image (Fig. 10b), $Aβ_{1-42}$ after incubation for 48 h at 37 °C, formed fully fledged, bulky and denser aggregates than $Aβ_{1-42}$ alone (Fig. 10a) at 0 h kept at 0 °C. Significantly fewer aggregates were observed in the positive control (curcumin) (Fig. 10c). Whereas, the aggregation inhibition results were distinctly seen with the addition of **P1** and **P3** (25 µM each), as sparse fibrils were noticed (Fig. 10d and e respectively), as compared to $Aβ_{1-42}$ alone (Fig. 10b). The TEM analysis results are consistent with the result of ThT binding assay, indicating compounds **P1** and **P3** to be very effective Aβ aggregation inhibitors.

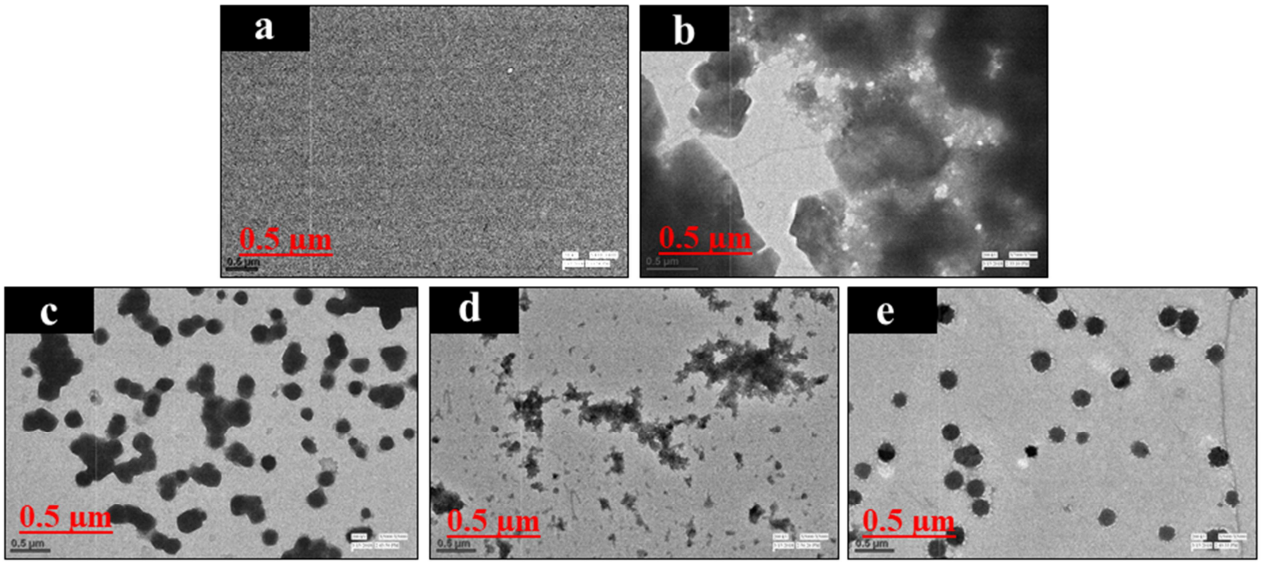

Fig. 10. TEM study of self-induced Aβ aggregation on co-incubating 25 µM Aβ with: (a) no compound at 0 °C, (b) no compound for 48 h at 37 °C, (c) 25 µM positive control curcumin at 37 °C for 48 h, (d) 25 µM compound **P1** at 37 °C for 48 h, and (e) 25 µM of **P3** at 37 °C for 48 h.

2.4.7. Evaluation of Copper-induced $Aβ_{1-42}$ Peptide Aggregation Inhibition

Cu (II) has been proved to form a complex with Aβ in a 1:1 ratio. The reported affinity of Aβ towards Cu (II) ranges from 10^{-18} to 10^{-6} M. It has been suggested that Cu (II) aids Aβ aggregation in some capacity. Despite the variability in the dissociation constants, it is understood that the affinity of Aβ towards Cu (II) is in a biologically relevant range. To examine the effect of Cu (II) on Aβ aggregation and subsequently the inhibition of the Aβ-Cu (II) complex by test compounds, a ThT assay was performed with **P1** and **P3** the most potent Aβ aggregation inhibitors. Table 6, details the fluorescence intensity by Aβ alone, Aβ with Cu(II), Aβ with Cu(II) and both the compounds (P1, P3) and with curcumin. It was observed that Cu (II) induces Aβ aggregation by 0.5 fold. The fluorescence spectra of Cu(II) ion showed negligible fluorescence intensity as shown in fig. 11 Hence this paramagnetic ion does not affect the fluorescence. Fluorescence value for peptide Aβ when treated with Cu^{2+} rose higher than Aβ alone (Fig. 12b) evidencing that this metal ion escalates aggregation of Aβ.

Fluorescence data for Aβ + Cu^{2+} + test compounds shows a decrease more than that of standard compound Curcumin (**P3**, 58.75 % inhibition; **P1**, 56.98 % inhibition and Curcumin, 45.18% inhibition) (Table. 6). The results convey that the tested molecules hold the capacity to restrain Copper-induced Aβ aggregation by chelation with Cu^{2+} ions.

Table 6. Fluorescence study of Copper-induced Aβ aggregation inhibition by **P1**, **P3** and Curcumin.

Sample	**Fluorescence intensity**
Aβ	412.33 ± 40.12
Aβ + Cu^{2+}	606.64 ± 36.11
Aβ + Cu^{2+} +**P1** (25uM)	260.95 ± 29.11
Aβ + Cu^{2+} +**P3** (25uM)	250.2 ± 24.98
Aβ + Cu^{2+} +Curcumin (25uM)	332.58 ± 32.99

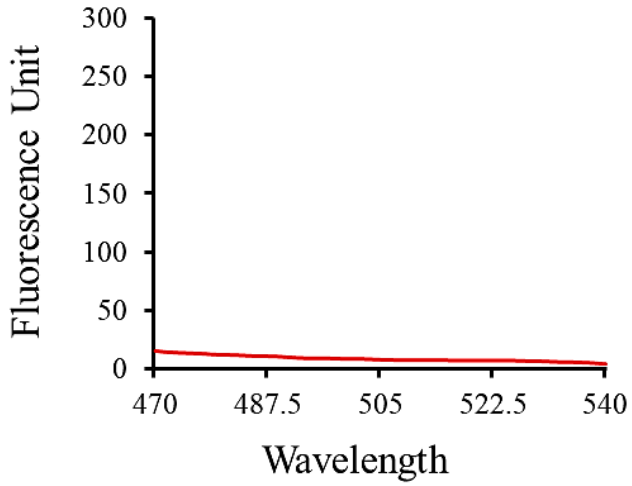

Fig. 11. Fluorescence intensity of Cu(II) alone.

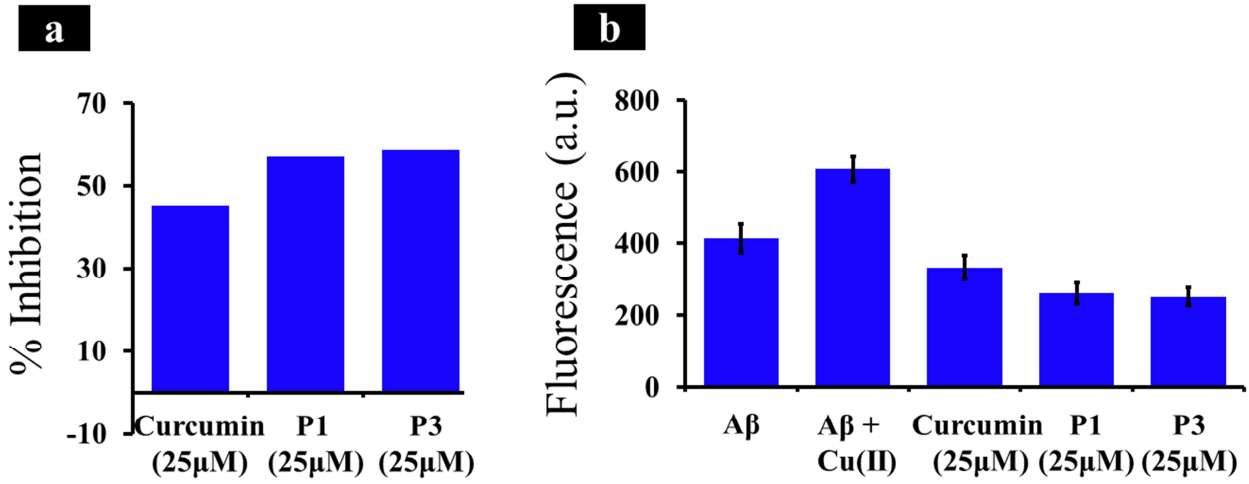

Fig. 12. (a) % inhibition (mean ± S.D) of Cu^{2+} induced $A\beta_{1-42}$ aggregation by Curcumin (25 μM), compound **P1** and **P3**; **(b)** ThT fluorescence intensity for Aβ alone, Aβ+ Cu^{2+}, Aβ+ Cu^{2+}+curcumin (25 μM), Aβ+ Cu^{2+}+compound **P1** (25 μM), and Aβ+ Cu^{2+}+compound **P3** (25 μM).

2.4.8. Antioxidant activity *in vitro* using oxygen radical absorbance capacity-fluorescein (ORAC-FL) method

A clearly noticeable characteristic found in brains of patients with AD is the oxidative stress. Production of free radicals has been implied in the process of neurodegeneration. Antioxidant

activity of all compounds was evaluated from ORAC-FL method [52] using trolox as the reference compound. This method works upon inhibition of oxyradical-induced oxidation of the 2, 2-azobis-(2-methylpropionamidine) dihydrochloride (AAPH) by antioxidant entity such as Trolox. Peroxyl radicals generated in a time-dependent fashion in the course of thermal disintegration of AAPH will suppress the fluorescence signal. Therefore a substance having antioxidant activity will consume peroxyl radicals and thus fluorescence diminution gets reduced according to its ORAC capacity. Results for antioxidant activity of **P1-P9** are depicted in Table 4. Antioxidation results ranged from 0.163 TE to 0.65 TE which suggests compounds do not possess significant antioxidant property in reference to the positive control Trolox. However to observe a subtituent-activity pattern, compound **P7** displays the best antioxidant property with 0.65 TE followed by compound **P9** (0.362 TE), which indicates that the bulkier substitutions to the N-(pyrazolo[3,4-b]pyridinyl)acetamide are disadvantageous.

2.4.9. Metal-chelating properties of compounds P1 and P3

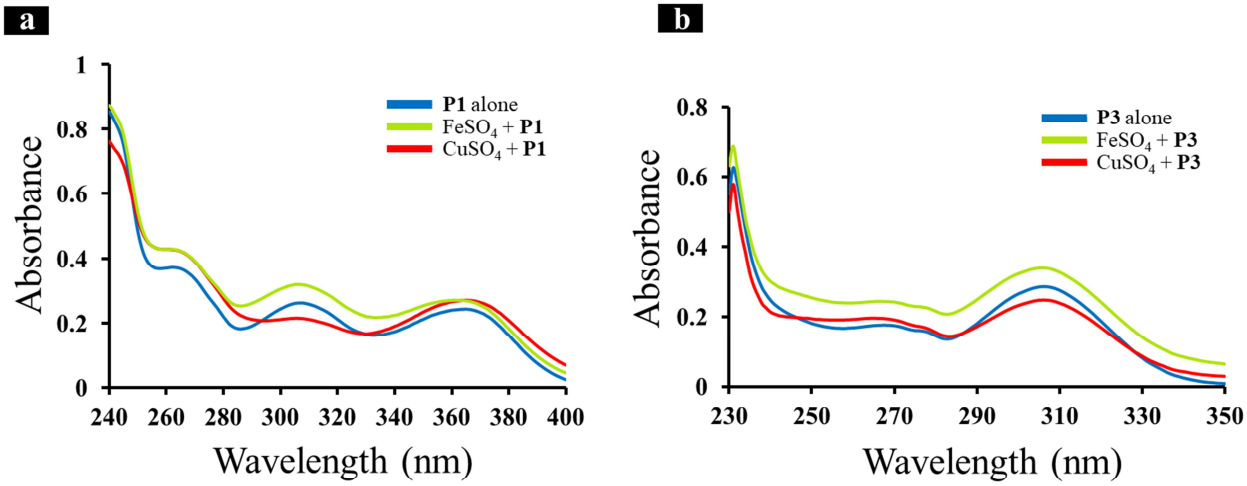

Fig. 13. (a) UV spectrum for **P1** alone (blue), in presence of Cu^{2+} (red) and in the presence of Fe^{2+} (green): (b) UV spectrum of **P3** alone (blue), in the presence of Cu^{2+} (red) and in the presence of Fe^{2+} (green)

The potential of test compounds **P1** and **P3** to chelate metals like $Fe^{2+}$and Cu^{2+} was explored using UV-Vis spectroscopy. Compound **P3** in the absence of metal ion gave a peak at 306 nm. On addition of $CuSO_4$, a decline in the absorbance was observed. This hypochromic shift alludes to the formation of P3-Cu (II) complex. On addition of $FeSO_4$ to compound, the compound displayed a hyperchromic shift at 306 nm. These changes in the absorbance suggest the binding of $CuSO_4$ and $FeSO_4$ to compound **P3**. The same shifts were observed for compound **P1** at 309 nm. Both compounds displayed a hypochromic shift in absorbance on addition of $CuSO_4$ and a hyperchromic shift on adding $FeSO_4$, suggesting the formation of compound-metal complex.

2.4.10. Prediction of activity spectra for substances

Table 7. Prediction of activity spectra for substances (PASS prediction) for the test inhibitors, Pa>0.50, considered as potent Nootropic.

Compounds	Nootropic	
	Pa[a]	**Pi**[b]
P1	0.74	0.03
P2	0.71	0.04
P3	0.82	0.01
P4	0.80	0.02
P5	0.77	0.02
P6	0.76	0.02
P7	0.81	0.01
P8	0.81	0.01
P9	0.86	0.01
Donepezil	0.749	0.028

[a] Pa is the estimate of probability to be active.

[b] Pi is the estimate of probability to be inactive.

Probable nootropic activity of novel piperazine analogues was predicted and analyzed *via* a computer program, PASS (prediction of activity spectra for substances). Pa and Pi are the estimates of probability to be active and inactive respectively. Based on the large probable

activity (Pa) values given by the PASS computer program the compounds were evaluated for their nootropic activity (Table 7). All the compounds display potent nootropic activity. Especially compounds **P3**, **P4**, **P5**, **P6**, **P7**, **P8** and **P9** show a significantly high nootropic activity at 0.816, 0.794, 0.768, 0.761, 0.815, 0.812 and 0.859 respectively in comparison to Donepezil (0.749).

2.4.11. ADMET and Toxicity prediction

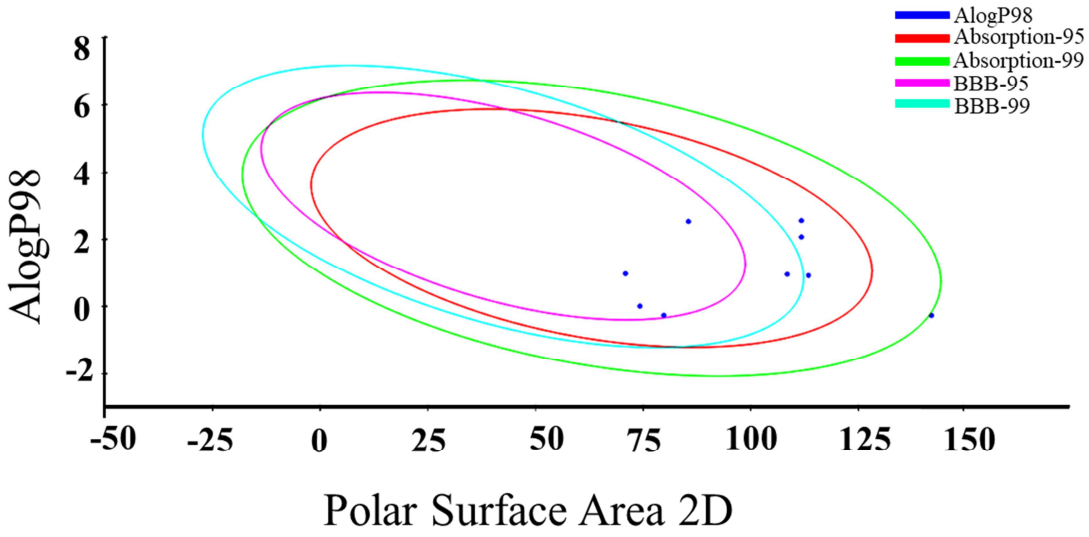

Fig. 14. Discovery Studio 4.0 (Accelrys, San Diego, CA) ADMET Descriptors, 2D PSA in A^0 for synthesized inhibitors plotted against corresponding calculated partition coefficient.

Absorption, distribution, metabolism, excretion, and toxicity (ADMET) are factors that are important players in drug development. Shortfall of efficacy and excess toxicity are associated to drug discovery failures. Adequate lipophilicity is requisite for the drugs to cross membrane and the cytosol to reach target. The ADMET-related properties given in tables S1-S2 are used to refine the drug likeness properties. ADMET properties of the test compounds were predicted *via* ADMET descriptors in Discovery Studio 2.1. and are summarized in Table S1-S2 in supplementary information. The module makes use of mathematical models, to theoretically

evaluate these characteristics using a set of rules which define threshold ADMET characteristics for specific molecular structure based on the available drug information. The prediction of absorption corresponds to the human intestinal absorption after oral administration. The extent of absorption for human intestinal absorption (HIA) model is defined by 95% and 99% confidence ellipses in polar surface area (PSA) (2D), AlogP98 plane. Plotted ellipses convey the areas having well-absorbed inhibitors. The blood brain barrier model predicts about the BBB penetration for compound after its oral administration. The 95% and 99% confidence ellipses in the PSA 2D, AlogP98 plane and blood-brain barrier penetration prediction were derived employing a quantitative linear regression model. The area enclosed by the ellipses is a prediction of good intestinal absorption and BBB with no violation of ADMET properties. Four of the test compounds were situated inside the four ellipses suggesting suitable absorption and BBB penetration. Well-absorbed compounds are found in the ellipse region. The BBB model predicts blood-brain penetration of compound after oral administration. Toxicity tests showed that most of the compounds were non-toxic, non-mutagenic and non-carcinogenic. The toxicity predictions are listed in table S2 in supplementary information. Furthermore the test compounds exhibited no skin irritancy and some ocular irritancy ranging from none to a severe one.

3. CONCLUSION

Our studies focused on assessing activity of 4-substituted piperazine-pyrazolo-pyridin-3-yl-acetamide analogues *in vitro* against important biological targets of Alzheimer's disease including, inhibition of AChE, Aβ aggregation/disaggregation, their antioxidant property to establish these compounds as multi target drug ligands. Anti-cholinesterase activity indicated that out of the screened inhibitors, five displayed better activity result than the standard drug Donepezil. Compounds **P7** and **P9** had a high inhibition potency for AChE (IC_{50} = 4.8 nM and

IC_{50} = 4.9 nM respectively). The compounds displayed a weak BuChE inhibition with most of the compounds giving an IC_{50} greater than 100 μM, therefore displaying high selectivity for AChE. The most selective compounds (**P7** and **P9**) showed selectivity greater than 20,000. Furthermore, kinetic study of **P3** showed that it was mixed type inhibitor. All tested compounds inhibited Aβ aggregation, compounds **P1** and **P3** evinced the most promising results (81.64% and 79.47% respectively). All the tested compounds were found to possess low antioxidant properties, displaying a lower potential to scavenge free radicals compared to trolox. ADMET and toxicity profiling predicted low toxicity for all the compounds. Overall compound **P3** could be further investigated as a lead molecule for future investigation towards Multi-Target Directed Ligand therapy.

4. Experimental section

4.1. Chemistry

All the chemical substances, reagents and solvents were brought from the commercial vendors such as Sigma Aldrich (St. Louis, MO, USA), Merck (Darmstadt, Germany), Alfa Aesar (Massachusetts) and Spectrochem Pvt. Ltd. (India). ^{1}H NMR spectra were observed on Bruker Avance 400 MHz spectrophotometer using deuterated solvent. Chemical shifts were displayed in δ (ppm) and tetramethylsilane was taken as internal standard. Mass spectra were recorded on an Agilent 6538 Ultra High Definition Accurate Mass-Q-TOF (LC-HRMS) instrument. Thin layer chromatography (TLC) analysis was achieved with Merck silica gel (60-120 and F254) Aluminum-coated TLC sheets of 0.25 mm thickness. Spots on these were seen with UV light at short (254 nm) and long (365 nm) wavelengths.

4.1.1. Procedure for Synthesis of 1H-pyrazolo[3,4-b]pyridin-3-amine (2)

In a round bottom flask 5 g (36 mmol) of 2-chloronicotinonitrile and 6 ml (38.25 mmol) hydrazine hydrate were mixed in ethanol. Reaction mixture was refluxed for 3-4 h and the reaction completion as well as formation of desired product was confirmed by TLC. After completion of reaction ethanol was eliminated under reduced pressure with the help of rota-evaporator. Thus obtained yellow solid was washed with ice cold water [53].

4.1.2. Method for preparation of 2-chloro-N-(1H-pyrazolo[3,4-b]pyridin-3-yl)acetamide (3)

To a stirring solution of sodium acetate in glacial acetic acid, 1H-pyrazolo[3,4-b]pyridin-3-amine (2.01g, 15 mmol) was added and the mixture was dissolved by mild heating. Then the reaction mixture was cooled to 0^{o} (ice-bath) and stoichiometric amount of chloroacetyl chloride was poured down dropwise over 1h, with continuous stirring. The stirring was continued for more 4 h, to give an orange solution with thick precipitate. The content was poured over crushed ice and filtered to give white solid.

White solid (50%); ^{1}H NMR (400 MHz, DMSO): δ (ppm) 13.33 (s, 1H, Ar-NH), 11.05 (s, 1H, CONH), 8.51 (dd, 1H, *J* = 8 Hz, Ar-H), 8.37 (d, 1H, *J*= 8 Hz, Ar-H), 7.17 (dd, 1H, *J* = 12 Hz, Ar-H), 4.37 (s, 2H, $COCH_2Cl$)

4.1.3. General procedure for synthesis of compound 4a, 4b

The diethyl 2-((phenylamino)methylene)malonates were synthesized by mixing diethyl (ethoxymethylene) malonate (25 mmol) and aniline or p-toluidine (25 mmol) in a round bottom flask. 6.5 ml benzene was added to it and it was refluxed for 1.5 h. reaction mixture was concentrated under vacuum and the crude obtained was left to crystallize at room temperature. Solid obtained was washed with hexane and dried [25].

4.1.4. General procedure for preparation of compound 5a, 5b

The respective ethyl 4-chloroquinoline-3-carboxylates from **4a** and **4b** were synthesized by heating compound 4a or 4b (85 mmol) with $POCl_3$ (1.34 mol) under reflux for 18 h. After the reaction mixture was cooled it was concentrated aand extracted with DCM (400 ml) and water (200 ml). sodium sulphate was used to dry the organic layer which was concentrated and purified by column chromatography (17% EtOAc/Hexane)[25].

4.1.5. General procedure for synthesis of compound 6a, 6b

The ethyl 4-(piperazin-1-yl)quinoline-3-carboxylates were prepared by mixing compound **5a**/**5b** with excess amount of piperazine (7 eq.) in anhydrous methanol and refluxing overnight at 60-70^{o}C. The reaction was monitored *via* TLC. On completion of reaction the organic solvent was concentrated on rota-evaporator and the crude product left was extracted using ethyl acetate (3x100 ml) and then with brine solution. The combined ethyl acetate layers were concentrated and the acquired crude products were purified *via* recrystallization from MeOH solvent.

4.1.6. General procedure for synthesis of compounds P1 and P2

2-chloro-N-(1H-pyrazolo[3,4-b]pyridin-3-yl)acetamide (**3**) (1g) was added to a solution of N-substituted piperazine derivatives **6a/6b** (4.3 mmol) and triethyl amine (5.7 mmol) in 20 mL THF (anhydrous). Reaction mixture was refluxed for 4hs and was monitored *via* TLC. On completion of reaction the solvent was concentrated on rota-evaporator and thus obtained crude product was extracted with the help of ethyl acetate (3x100 ml) and then with brine solution. Combined ethyl acetate layers were concentrated and the acquired crude products were purified *via* recrystallization in methanol solvent.

4.1.6.1. *Ethyl 4-(4-(2-((1H-pyrazolo[3,4-b]pyridin-3-yl)amino)-2-oxoethyl)piperazin-1-yl)quinoline-3-carboxylate (**P1**)*

White solid (48%); ^{1}H NMR (400 MHz, $CDCl_3$): δ (ppm) 13.34 (s, 1H, Ar-NH), 10.81 (s, 1H, CONH), 8.81 (ss, 1H, Ar-H), 8.51 (d, 1H, *J* = 4 Hz, Ar-H), 8.43 (d, 1H, *J*= 8 Hz, Ar-H), 8.22 (d, 1H, *J* = 8 Hz, Ar-H), 8.02 (d, 1H, *J* = 8 Hz, Ar-H), 7.82 (t, 1H, *J* = 12 Hz, Ar-H), 7.67 (t, 1H, *J* = 20 Hz, Ar-H), 7.18 (t, 1H, *J* = 12 Hz, Ar-H), 4.45 (q, 2H, *J* = 20 Hz, CH_2), 3.42 (s, 2H, $COCH_2N$), 3.42 (s, 4H, NCH_2), 3.15 (s, 4H, NCH_2), 1.39 (t, 3H, *J* = 12 Hz, CH_3); ^{13}C NMR (100 MHz,$CDCl_3$) δ 167.83, 155.49, 152.78, 151.08, 150.50, 150.32, 139.72, 133.39, 131.79, 130.41, 127.79, 125.51, 125.26, 119.14, 116.97, 108.68, 62.53, 53.78, 51.17, 41.06, 40.86, 40.65, 40.44, 40.23, 40.02, 39.81, 15.08; HRMS in MeOH for $C_{24}H_{25}N_7O_3$ (Mol. wt = 459.5004 g mol^{-1}) (ESI, m/z): observed, 460.2093: calculated, 460.2097 $[M + H]^+$.

4.1.6.2. *Ethyl 4-(4-(2-((1H-pyrazolo[3,4-b]pyridin-3-yl)amino)-2-oxoethyl)piperazin-1-yl)-6-methylquinoline-3-carboxylate (**P2**)*

White solid (50%); ^{1}H NMR (400 MHz, $CDCl_3$): δ (ppm) 13.28 (s, 1H, Ar-NH), 10.43 (s, 1H, CONH), 8.70 (s, 1H, Ar-H), 8.50 (d, 1H, *J* = 4 Hz, Ar-H), 8.41 (d, 1H, *J* = 12 Hz, Ar-H), 7.93 (s, 1H, Ar-H), 7.91 (d, 1H, *J* = 8 Hz, Ar-H), 7.64 (d, 1H, *J* = 8 Hz, Ar-H), 7.16-7.13 (dd, 1H, Ar-H), 4.43 (q, 2H, *J* = 2 Hz, OCH_2), 3.41 (s, 2H, $COCH_2N$), 2.88 (d, 4H, NCH_2), 2.54 (s, 3H, Ar-CH_3), 2.50 (d, 4H, NCH_2), 1.38 (t, 3H, *J* = 16 Hz, Aliph-CH_3); ^{13}C NMR (100 MHz,$CDCl_3$) δ 168.65, 167.95, 155.56, 152.75, 150.54, 150.23, 149.36, 140.16, 137.04, 134.59, 133.30, 130.36, 125.66, 123.52, 119.29, 117.21, 108.76, 77.80, 77.49, 77.17, 62.45, 62.31, 54.70, 51.76, 22.63, 14.97; HRMS in MeOH for $C_{25}H_{27}N_7O_3$ (Mol. wt = 473.5270 g mol^{-1}) (ESI, m/z): observed, 474.2209: calculated, 474.2254 $[M + H]^+$.

4.1.7. General procedure for preparation of compound P3

2-chloro-N-(1H-pyrazolo[3,4-b]pyridin-3-yl)acetamide (**3**) (1g) was added to a solution piperazine (2.37 mmol) and triethyl amine (5.7 mmol) in 20 mL THF (anhydrous). The reaction

mixture was refluxed for 4hs and the reaction was monitored *via* TLC. On termination of reaction the solvent was concentrated on rota-evaporator and the crude product was extracted using ethyl acetate (3x100 ml) followed by brine solution. The combined layers of organic solvent were concentrated and the acquired crude products were purified by recrystallization in methanol solvent.

4.1.7.1. *2,2'-(piperazine-1,4-diyl)bis(N-(1H-pyrazolo[3,4-b]pyridin-3-yl)acetamide) (**P3**)*

White solid (55%); ^{1}H NMR (400 MHz, $CDCl_3$): δ (ppm) 13.28 (s, 2H, Ar-NH), 10.47 (s, 1H, CONH), 10.32 (s, 1H, CONH), 8.49-8.35 (m, 4H, Ar-H), 7.14 (t, 2H, *J*= 8 Hz, Ar-H), 3.89 (s, 4H, $COCH_2N$), 2.80 (s, 4H, NCH_2), 2.47 (s, 4H, NCH_2); ^{13}C NMR (100 MHz,$CDCl_3$) δ 169.13, 165.04, 157.59, 154.74, 152.78, 150.50, 150.22, 140.00, 133.45, 116.88, 108.83, 108.69, 95.59, 61.63, 61.22, 53.61, 52.83, 48.49, 41.05, 40.84, 40.63, 40.42, 40.21, 40.00, 39.79; HRMS in MeOH for $C_{20}H_{22}N_{10}O_2$ (Mol. wt = 434.4545 g mol^{-1}) (ESI, m/z): observed, 457.1821: calculated, 457.1825 $[M + Na]^+$.

4.1.8. Method of preparation of compound 8

For the synthesis of 5-Methyl-[1,2,4]triazolo[1,5-a]pyrimidin-7-ol (**8**), ethylacetoacetate (25 mmol) and 3-amino-1,2,4-triazole (25 mmol) in 12 ml acetic acid was refluxed for 4 h. Precipitate formed was cooled, filtered, and washed with chilled acetic acid, followed by ethanol. It was dried and used for further reaction [25].

4.1.9. Method of preparation of compound 9

For the synthesis of 7-Chloro-5-methyl-[1,2,4]triazolo[1,5-a]pyrimidine (**9**), phosphorous oxychloride (30 mmol) was added to compound 8 (10 mmol) and refluxed for 1-2 h. After the reaction was complete it was allowed to cool to room temperature and then remaining $POCl_3$ was

removed at reduced pressure. Crude sample was triturated with chilled water. Compound was extracted using DCM and purified via column chromatography (60% EtOAc/hexane) [25].

4.1.10. Method of preparation of compound 10

For the synthesis of 5-methyl-7-(piperazin-1-yl)-[1,2,4]triazolo[1,5-a]pyrimidine (**10**), piperazine (10 mmol), compound 9 (10 mmol) and potassium carbonate (12 mmol) were refluxed in 1,4-dioxane at 100 ^{o}C for 3h. After the reaction was complete, reaction mixture was filtered and the filtrate was concentrated on rota vapour [25].

4.1.11. Method of preparation of compound P4

2-chloro-N-(1H-pyrazolo[3,4-b]pyridin-3-yl)acetamide (**3**) (1g) was added to a solution of 1-{5-methyl-[1,2,4]triazolo[1,5-a]pyrimidin-7-yl}piperazine (**10**) (4.3 mmol) and triethyl amine (5.7 mmol) in 20 mL THF (anhydrous). The reaction mixture was refluxed for 4hs and the reaction was observed *via* TLC. On reaction completion the solvent was concentrated on rota-evaporator and the crude product was extracted using ethyl acetate (3x100 ml) followed by brine solution. The combined layers of organic solvent were concentrated and the acquired crude products were purified by recrystallization in methanol solvent.

*4.1.11.1. 2-(4-(5-methyl-[1,2,4]triazolo[1,5-a]pyrimidin-7-yl)piperazin-1-yl)-N-(1H-pyrazolo[3,4-b]pyridin-3-yl)acetamide (**P4**)*

White solid (70%); ^{1}H NMR (400 MHz, DMSO): δ (ppm) 13.28 (s, 1H, Ar-NH), 10.47 (s, 1H, CONH), 8.49 (d, 1H, *J* = 4 Hz, Ar-H), 8.42 (s, 1H, Ar-H), 8.37 (d, 1H, *J* = 8 Hz, Ar-H), 7.14 (t, 1H, *J* = 12 Hz, Ar-H), 6.57 (s, 1H, Ar-H), 3.90 (t, 4H, NCH_2), 3.36 (s, 2H, $COCH_2N$), 2.80 (t, 4H, NCH_2), 2.48 (ss, 3H, CH_3); ^{13}C NMR (100 MHz,$CDCl_3$) δ 169.13, 165.05, 157.60, 154.74, 152.78, 150.51, 150.22, 140.00, 133.45, 116.89, 108.83, 95.60, 61.21, 52.83, 48.49, 41.05, 40.84,

40.63, 40.42, 40.22, 40.01, 39.80, 25.49; HRMS in MeOH for $C_{18}H_{20}N_{10}O$ (Mol. wt = 392.4178 g mol^{-1}) (ESI, m/z): observed, 415.1722: calculated, 415.1719 $[M + Na]^+$.

4.1.12. Method of synthesis of 7-chloro-4-(piperazin-1-yl)quinoline (11)

The 7-Chloro-4-piperazin-1-yl-quinoline was synthesized by a known procedure [54].

4.1.13. Methods of preparation of compound P5

2-chloro-N-(1H-pyrazolo[3,4-b]pyridin-3-yl)acetamide (**3**) (1g) was added to a solution 7-chloro-4-(piperazin-1-yl)quinoline (**11**) (4.3 mmol) and triethyl amine (5.7 mmol) in 20 mL THF (anhydrous). The reaction mixture was refluxed for 4hs and was monitored *via* TLC. On completion of reaction the solvent was concentrated using rota-evaporator and the crude product was extracted *via* ethyl acetate (3x100 ml) and then with brine solution. The combined organic layers were concentrated and acquired crude products were purified *via* recrystallization in methanol solvent.

*4.1.13.1. 2-(4-(7-chloroquinolin-4-yl)piperazin-1-yl)-N-(1H-pyrazolo[3,4-b]pyridin-3-yl)acetamide (**P5**)*

White solid (78%); ^{1}H NMR (400 MHz, DMSO): δ (ppm) 13.27 (s, 1H, Ar-NH), 10.45 (s, 1H, CONH), 8.72 (d, 1H, *J* = 4 Hz, Ar-H), 8.50 (d, 1H, *J* = 4 Hz, Ar-H), 8.40 (d, 1H, *J* = 12 Hz, Ar-H), 8.06 (d, 1H, *J* = 8 Hz, Ar-H),7.99 (s, 1H, Ar-H), 7.58 (dd, 1H, Ar-H), 7.17 (dd, 1H, Ar-H), 7.05 (d, 1H, *J* = 8 Hz, Ar-H), 3.41 (s, 2H, $COCH_2N$), 3.28 (t, 4H, NCH_2), 2.90 (t, 4H, NCH_2). ^{13}C NMR (100 MHz, DMSO) δ 169.16, 157.22, 153.08, 152.81, 150.56, 150.21, 140.04, 134.48, 133.50, 128.97, 126.98, 126.67, 122.31, 116.87, 110.36, 108.78, 80.20, 79.87, 79.54, 61.46, 53.42, 52.65, 41.09, 40.88, 40.67, 40.46, 40.26, 40.05, 39.84; HRMS in MeOH for $C_{21}H_{20}ClN_7O$ (Mol. wt = 421.8828 g mol^{-1}) (ESI, m/z): observed, 444.1314: calculated, 444.1316 $[M + Na]^+$.

4.1.14. General methods of preparation of 2-(piperazin-1-yl)nicotinonitrile (12)

The 2-(piperazin-1-yl)nicotinonitrile was prepared according to the general procedure of synthesis of compounds 6a, 6b.

4.1.13. Procedure for preparation of compound P6

2-chloro-N-(1H-pyrazolo[3,4-b]pyridin-3-yl)acetamide (**3**) (1g) was added to a solution 2-(piperazine-1-yl)pyridine-3-carbonitrile (**12**) (4.3 mmol) and triethyl amine (5.7 mmol) in 20 mL of anhydrous THF. The reaction mixture was refluxed for 4hs and the reaction was monitored *via* TLC. On termination of reaction the solvent was concentrated on rota-evaporator and the crude product was extracted using ethyl acetate (3x100 ml) and then with brine solution. The combined organic layers were concentrated and the acquired crude products were purified by recrystallization in methanol solvent.

4.1.13.1. *2-(4-(3-cyanopyridin-2-yl)piperazin-1-yl)-N-(1H-pyrazolo[3,4-b]pyridin-3-yl)acetamide* ***(P6)***

White solid (74%); ^{1}H NMR (400 MHz, DMSO): δ (ppm) 13.28 (s, 1H, Ar-NH), 10.43 (ss, 1H, CONH), 8.49 (d, 1H, *J* = 4 Hz, Ar-H), 8.41 (m, 2H, Ar-H), 8.07 (dd, 1H, *J* = 8 Hz, Ar-H), 7.16-7.13 (dd, 1H, *J* = 12 Hz, Ar-H), 6.93 (dd, 1H, *J* = 12 Hz, Ar-H), 3.68 (d, 4H, NCH_2), 3.33 (s, 2H, $COCH_2N$), 2.73 (d, 4H, NCH_2); ^{13}C NMR (100 MHz, DMSO) δ ; 169.24, 161.16, 152.99, 152.74, 150.23, 145.24, 139.98, 133.45, 118.79, 116.93, 115.62, 108.86, 95.31, 61.38, 53.27, 48.73, 40.96, 40.75, 40.54, 40.34, 40.13, 39.92, 39.71; HRMS in MeOH for $C_{18}H_{18}N_8O$ (Mol. wt = 362.3885 g mol^{-1}) (ESI, m/z): observed, 385.1504: calculated, 385.1501 $[M + Na]^+$.

4.1.14. Method for the synthesis of compounds P7-P9

2-chloro-N-(1H-pyrazolo[3,4-b]pyridin-3-yl)acetamide (**3**) (1g) was added to a solution containing morpholine/piperidine/4-methylpiperazine (4.7 mmol) in 20 mL THF (anhydrous). The reaction mixture was refluxed for 1h and the reaction was monitored *via* TLC. As the

reaction completed the solvent was concentrated on rota-evaporator and the crude product was extracted using ethyl acetate solvent (3x100 ml) and then twice with brine solution. Combined organic layers were concentrated and the acquired crude products were purified by recrystallization in methanol solvent.

4.1.14.1. *2-(piperidin-1-yl)-N-(1H-pyrazolo[3,4-b]pyridin-3-yl)acetamide (**P7**)*

White solid (48%): ^{1}H NMR (400 MHz, $CDCl_3$): δ (ppm) 13.29 (s, 1H, Ar-NH), 10.50-10.49 (dd, 1H, *J* = 4 Hz, Ar-H), 8.39 (d, 1H, *J* = 8 Hz, Ar-H), 7.16-7.13 (dd, 1H, *J* = 4 Hz, Ar-H), 3.40 (d, 4H, NCH_2), 2.69 (s, 2H, $COCH_2N$), 1.62 (d, 4H, *J* = 8 Hz, CH_2), 1.43 (s, 2H, CH_2); ^{13}C NMR (100 MHz, DMSO) δ; 152.78, 150.29, 139.78, 133.42, 116.94, 108.62, 99.17, 61.42, 54.76, 41.08, 40.87, 40.66, 40.45, 40.24, 40.03, 39.82, 25.74, 23.89; HRMS in MeOH for $C_{13}H_{17}N_5O$ (Mol. wt = 259.3070 g mol^{-1}) (ESI, m/z): observed, 260.1538: calculated, 260.1511 $[M + H]^+$.

4.1.14.2. *2-Morpholino-N-(1H-pyrazolo[3,4-b]pyridin-3-yl)acetamide (**P8**)*

Cream coloured solid (75%): ^{1}H NMR (400 MHz, $CDCl_3$): δ (ppm) 13.26 (s, 1H, Ar-NH), 10.35 (s, 1H, CONH), 8.49 (d, 1H, *J* = 4 Hz, Ar-H), 8.37 (d, 1H, *J* = 8 Hz, Ar-H), 7.15-7.12 (dd, 1H, Ar-H), 3.64 (t, 4H, OCH_2), 3.24 (s, 2H, $COCH_2N$), 2.56 (t, 4H, *J* = 8 Hz, NCH_2); ^{13}C NMR (100 MHz,$CDCl_3$) δ 168.20, 151.88, 149.31, 139.10, 132.56, 115.98, 107.90, 66.17, 61.05, 53.17, 40.15, 39.94, 39.73, 39.52, 39.31, 39.10, 38.89; HRMS in MeOH for $C_{12}H_{15}N_5O_2$ (Mol. wt = 261.2798 g mol^{-1}) (ESI, m/z): observed, 284.1125: calculated, 284.1123 $[M + Na]^+$.

4.1.14.3. *(4-methylpiperazin-1-yl)-N-(1H-pyrazolo[3,4-b]pyridin-3-yl)acetamide (**P9**)*

Colourless crystals (68%); ^{1}H NMR (400 MHz, $CDCl_3$): δ (ppm) 13.25 (s, 1H, Ar-NH), 10.26 (s, 1H, CONH), 8.49 (d, 1H, *J*= 4 Hz, Ar-H), 8.38 (d, 1H, *J*= 8 Hz, Ar-H), 7.15-7.12 (dd, 1H, Ar-

H), 3.22 (s, 2H, $COCH_2N$), 2.56 (s, 4H, NCH), 2.38 (s, 4H, NCH), 2.19 (ss, 3H, NCH_3); ^{13}C NMR (100 MHz,$CDCl_3$) δ 169.21, 152.80, 150.22, 139.99, 133.51, 116.87, 108.66, 61.65, 55.56, 53.58, 46.66, 41.07, 40.86, 40.66, 40.45, 40.24; HRMS in MeOH for $C_{13}H_{18}N_6O$ (Mol. wt = 274.3216 g mol^{-1}) (ESI, m/z): observed, 275.1616: calculated, 275.1620 $[M + H]^+$.

4.2. Docking protocol

To demonstrate the interaction mechanism of synthesized compounds with $A\beta_{1-42,}$ 3D crystallographic structure for $A\beta_{1-42}$ peptide (PDB ID: 1IYT) was extracted from PDB (www.rcsb.org) [55]. $A\beta_{1-42}$ and ligands were saved in format of pdbqt in order to analyze the docking study. Docking of compounds with receptor $A\beta_{1-42}$ was done with AutoDock 4.2 using standard protocol. The protein-ligands interactions were performed *via* application of Lamarckian genetic algorithm [56]. Using the best free binding energy as well as the docking orientations within the range of 2.0 Å in RMSD tolerance, the molecules were clustered and ranked accordingly. The software PyMOL was used to see the ligand and receptor interactions at molecular level. All calculations were carried out on cmd.exe command window system.

Docking of synthesized compounds with acetylcholinesterase were carried out using Pardock [57] software. Bappl scoring function [58] was used for scoring of these docked structures. A complete protocol for docking was described elsewhere [59]. Herein, we had also used PyMOL [60] software to visualize molecular interactions between ligand and receptor.

4.3. Procedure for X-ray Crystallographic study

Crystal structure of synthesized compounds **P6** and **P9** were obtained *via* single-crystal X-ray di□raction method. The slow evaporation of methanol solutions of compounds **P6** and **P9** gave the colorless crystals that were boarded upon loops having mineral oil. An automated Bruker SMART APEX CCD di□ractometer having fine focus sealed tube (1.75 kW) Mo Kα X-ray

source (λ = 0.71073 Å) with elevating ω (width of 0.3° per frame) at 5 s frame^{-1} scanning speed was used to get the geometric data and intensity data *via* the ω-2θ scan mode and then corrected for Lorentz-polarization and absorption e□ects [61]. WinGx (version 1.63.04a) was utilised to solve as well as refine the structures *via* SHELXL-2013 method [62]. All non-hydrogen atoms were refined with anisotropic displacement coe□cients and non-hydrogen atom coordinates were permitted to be on their corresponding carbon atoms. The final refinement consisted of atomic positions of all atoms, isotropic thermal parameters for hydrogen atoms, and anisotropic thermal parameters for non-hydrogen atoms. The structural views of compounds P6 and P9 were procured with ORTEP [63]. Further details like crystallographic parameters; bond distances, and angles data are given in Table 1. The CCDC deposition numbers for **P6** is 1870982 and **P9** is 1870983.

4.4. Biological Evaluation

4.4.1. *In vitro* AChE and BuChE inhibition study

The spectroscopic method of Ellman et al. [64] was utilized to evaluate the AChE and BuChE inhibition for all synthesized inhibitors. Acetylcholinesterase (AChE, E.C. 3.1.1.7, *electric eel*), Butyrylcholinesterase (BuChE, E.C. 3.1.1.8, equine serum), Donepezil, acetylthiocholine (ATC) iodide, butyrylthiocholine (BTC) iodide and 5,5'-dithiobis-(2-nitrobenzoic acid) (Ellman's reagent, DTNB) were brought from Sigma Aldrich. The stock solutions were prepared in water and DMSO by adding test compounds to yield final test concentrations 0.01-100 µM. Preparation of enzyme solutions was carried out by dissolving lyophilized powder in autoclaved water. The assay medium comprised of 195 µL of 1 M phosphate buffer KH_2PO_4/K_2HPO_4 (pH 8.0), 5 µL of AChE (0.22 U/mL) or 5 µL of BuChE (0.06 U/mL) and 25 µl of different concentrations of synthesized inhibitors that were allowed to stand 5 min before 20 µL DTNB

(0.01 M) was added. Donepezil was taken as a positive control in same range of concentrations. Reaction was initiated by adding 4 µL of the 0.075 M substrate solution (ATC/BTC). After 5 minutes of adding the substrate the absorption was recorded at 412 nm, at 25 °C.

4.4.2. Kinetic characterization of AChE inhibitory activity

The kinetic characterization of the type of AChE inhibition by synthesized inhibitor was obtained by constructing reciprocal plot of 1/velocity versus 1/substrate at comparatively low concentrations of substrate *via* Ellman's method. Tested compound was studied at three concentrations of 10, 20, and 40 nM. Calculation of Km and Vmax values of the Michaelis–Menten kinetics were done by nonlinear regression from substrate–velocity curves with the help of Graph Pad Prism 5 software (San Diego, CA, USA). Linear regression was utilized in calculation of the Lineweaver–Burk plots.

4.4.3. Self-mediated $A\beta_{1-42}$ aggregation assay

To avoid self-aggregation of peptides ($A\beta_{1-42}$) they were initially mixed with hexafluoroisopropanol (HFIP) at a concentration of 8 mg/ml. The clearly dissolved peptide was then aliquoted in microcentrifuge tube. HFIP was removed by evaporation under a nitrogen stream to form a clear film in test tube. For the preparation of stable Aβ stock solution (5 mM), the pretreated $A\beta_{1-42}$ peptide samples were dissolved in the DMSO solvent. For the inhibition of self-induced Aβ aggregation, the dilution of Aβ stock solution was carried out with phosphate buffer (50 mM, pH 7.4) mediated $A\beta_{1-42}$ aggregation experiment. The mixture of peptides (10 µl, 100 µM, final concentration) in presence or absence of the synthesized inhibitors (25 µM) was incubated for 48 h at 37 °C.

4.4.4. Disaggregation of self-induced $A\beta_{1-42}$ aggregation

For disaggregation studies of self-mediated Aβ aggregation by test compounds, dilution of Aβ stock solution was carried out by using phosphate buffer (50 mM, pH 7.4). The mixture of the peptide (10 µl, 100 µM as final concentration) was incubated for 48 h at 37^{o} C, following which the compounds or buffer were added and incubated for 24 h at 37^{o} C. The measuring of the amyloid fibril formation was done *via* thioflavin-T fluorescence method [65,66]. Furthermore experiment with blanks containing phosphate buffer (50 mM. pH 7.4) instead of Aβ in presence or absence of test compounds was also conducted. As the incubation was complete the dilution of samples were done to 200 µl (final volume) using glycine-NaOH buffer (50 mM, pH 8.0).

4.4.5. Concentration dependent study of Aβ self-aggregation assay

For the concentration dependent Aβ self-aggregation experiment the stock solution of Aβ was diluted using phosphate buffer (50 mM, pH 7.4). The peptide (10 µl, 100 µM, final concentration) with or without the inhibitor (10, 15, 20 and 25 µM) was incubated for 48 h at 37 °C. Measurement of amyloid fibrils formation was done by the Th-T fluorescence method. Experiment on blanks reaction mixture containing phosphate buffer (50 mM, pH 7.4) instead of Aβ in presence or absence of test compounds was also performed. After incubation samples were diluted with glycine-NaOH buffer (50 mM, pH 8.0) to a final volume of 200 µl.

4.4.6. Inhibition of $A\beta_{1-42}$ fibril formation studied by TEM assay

Incubation of $A\beta_{1-42}$ (100 µM) dissolved in phosphate buffer (50 mM, pH 7.4) was done with and without inhibitors P1 and P3 (25 µM) at a temperature of 37 °C, 48 h. 10 µL of sample was kept on carbon grid followed by a minute incubation at RT. Grids were washed with double distilled water and finally stained by sodium phosphotungstate (PTS). The negatively stained compounds were then monitored by TEM (JEOL JEM-1400).

4.4.7. Study of the effects of P1 and P3 on Cu-induced $A\beta_{1-42}$ peptide aggregation

The effect of compounds P1 and P3 in Cu-mediated $A\beta_{1-42}$ aggregation inhibition experiment was studied by ThT fluorescence assay. The Aβ stock solutions were diluted with HEPES (20 μM, pH 6.6) containing 150 μM NaCl. The mixture of peptide (10 μL, 100 μM, final concentration) with or without copper (100 μM, final concentration) was incubated for 48 h at 37 °C. The compounds (25 μM, final concentration) were added and incubated for 24 h at 37 °C. After incubation 20 μL of the sample was diluted to a final volume of 200 μL with glycine−NaOH buffer (50 mM, pH 8.0) containing thioflavin T (5 μM).

4.4.8. Antioxidant activity by oxygen radical absorbance capacity (ORAC-FL) assay

The oxygen radical absorbance capacity-fluorescein (ORAC-FL) assay was used to learn the antioxidant capability of all test molecules. Chemicals used herein such as Trolox ((±)-6-hydroxy-2,5,7,8-tetramethylchromane-2-carboxylic acid), AAPH (2,2'-Azobis-(amidinopropane) dihydrochloride) and Fluorescein (FL) were brought from Sigma-Aldrich. The assay reactions involved the use of phosphate buffer (75 mM, pH 7.4) with reaction mixture to be 200 μL as final volume. 20 μL antioxidant and 120 μL FL (70 nM as final concentration) solutions were kept in a black 96-well microplate (96F untreat, Nunc). Reaction mixture was preincubated (15 min) at a temperature of 37 °C. AAPH solution (60 μL, 12 mM, final concentration) was poured in it with the help of a multichannel pipette and immediately placed this microplate in reader. Sample measurements were done for eight concentrations (1–8 μM). Fluorescence was measured for 80 minutes with emission at 520 nm and excitation at 485 nm. For each sample minimum three individual runs were performed. The fluorescence vs time graphs (antioxidant curves) were normalized to the curve of the blank (without antioxidant). Net area under the fluorescence decay

curve (AUC) for a sample was evaluated by subtracting the AUC regarding blank. The regression equations among net AUC and antioxidant concentration were calculated for every sample. The ORAC-FL value of all samples was evaluated with the use of the standard curve, which is thus expressed as Trolox equivalents. ORAC-FL value was taken as 1 for Trolox.

4.4.9. Metal chelation studies

Study of metal binding was performed using a Perkin-Elmer Multimode Reader (Thermo Scientific). The UV absorption of the synthesized compounds **P1** and **P3** (30 μM, final concentration) alone or with $CuSO_4$ and $FeSO_4$ (30 μM, final concentration) in 20% (v/v) ethanol/buffer (150 mM NaCl, 20 mM HEPES, pH 7.4) was recorded for 30 min with wavelength ranging from 200 to 500 nm. The reaction mixture had a final volume of 700 μL.

4.4.10. ADME characteristic prediction and the TOPKAT analysis

The Absorption, Metabolism, Distribution and excretion properties of P1-P9 were predicted *via* Accelrys Discovery studio 4.0. It estimates the bioavailability of synthesized inhibitors. Parameters like PSA, solubility level, predicted aqueous solubility level and percent human oral absorption level were calculated. TOPKAT module of Accelrys Discovery studio 4.0 was used to perform virtual toxicity risk assessment. It calculates probable toxicity for a particular chemical structure by employing a range of cross-validated Quantitative Structure Toxicity Relationship (QSTR) models. The pyrazolopyridine-piperazine hybrids were examined for dose dependent toxicity parameters like FDA and NTP rodent carcinogen models, ocular irritancy, skin irritancy, developmental toxicity potential, mutagenicity and aerobic biodegradability.

CONFLICT OF INTEREST

The authors declare that there is no conflict of interest.

ACKNOWLEDGEMENTS

T.U. would like to acknowledge the financial support from University Grants Commission, India for the Basic Scientific Research (BSR-SRF) fellowship. Author S.S. is grateful to Ministry of AYUSH for the financial support (JRF). M.T. pays her thanks to the University of Delhi for sanctioning research funds to conduct the study.

REFERENCES

[1] G. McKhann, D. Drachman, M. Folstein, R. Katzman, D. Price, E.M. Stadlan, Clinical Diagnosis of Alzheimer's Disease Report of the NINCDS-ADRDA Work Group* under the Auspices of Department of Health and Human Services Task Force on Alzheimer's Disease. Neurology 34 (1984) 939-939.

[2] C. Patterson, The World Alzheimer Report 2018 'The state of the art of dementia research: New frontiers', Alzheimer's Disease International (ADI), London, 2018.

[3] A. Castro, A. Martinez, Targeting Beta-Amyloid Pathogenesis Through Acetylcholinesterase Inhibitors, Curr. Pharm. Des. 12 (2006) 4377-4387.

[4] C. Geula, M.M. Mesulam, Cortical cholinergic fibers in aging and Alzheimer's disease: a morphometric study, Neuroscience. 33 (1989) 469–481.

[5] A. Gella, N. Durany, "Oxidative stress in Alzheimer disease," Cell Adhesion and Migration, 3 (2009) 88–93.

[6] E. Scarpini, P. Scheltens, H. Feldman, Treatment of Alzheimer's disease: Current status and new perspectives, Lancet Neurol. 2 (2003) 539–547.

[7] M. Rosini, Polypharmacology: the rise of multitarget drugs over combination therapies, Future Med. Chem. 6 (2014) 485–487.

[8] Y. Huang, L. Mucke, Alzheimer mechanisms and therapeutic strategies, Cell, 148 (2012) 1204–1222.

[9] M. Citron, Alzheimer's disease: strategies for disease modification, Nat. Rev. Drug Discovery 9 (2010) 387–398.

[10] C. Haass and D. J. Selkoe, Soluble protein oligomers in neurodegeneration: lessons from the Alzheimer's amyloid beta-peptide, Nat. Rev. Mol. Cell Biol. 8 (2007) 101–112.

[11] D. J. Selkoe, Translating cell biology into therapeutic advances in Alzheimer's disease, Nature 399 (1999) A23–A31.

[12] S. Oddo, A. Caccamo, M. Kitazawa, B.P. Tseng, F.M. LaFerla, Amyloid deposition precedes tangle formation in a triple transgenic model of Alzheimer's disease, Neurobiol. Aging 24 (2003) 1063–1070.

[13] D.J. Selkoe, Alzheimer's disease: a central role for amyloid, J. Neuropathol. Exp. Neurol. 53 (1994) 438–447.

[14] C.J. Pike, D. Burdick, A.J. Walencewicz, C.G. Glabe, C.W. Cotman, Neurodegeneration induced by beta-amyloid peptides *in vitro*: the role of peptide assembly state, J. Neurosci. 13 (1993) 1676–1687.

[15] C. Zussy, A.Brureau, B. Delair, S. Marchal, E. Keller, G. Ixart, G. Naert, J. Meunier, N. Chevallier, T. Maurice, Time-course and regional analyses of the physiopathological changes induced after cerebral injection of an amyloid β fragment in rats, Am. J. Pathol. 179 (2011) 315–334.

[16] A. Blokland, Acetylcholine: A neurotransmitter for learning and memory? Brain Res. Brain Res. Rev. 21 (1995) 285-300.

[17] D.M. Quinn, Acetylcholinesterase: enzyme structure reaction dynamics and virtual transition states, Chem. Rev. 87 (1987) 955–979.

[18] P. Taylor, Z. Radic, The cholinesterases: from genes to proteins. Annu. Rev. Pharmacol. 34 (1994) 281–320.

[19] F. Massoud, S. Guathier, Update on the pharmacological treatment of Alzheimer's disease, Curr. Neuropharmacol. 8 (2010) 69–80.

[20] G. Benzi, A. Moretti, Is there a rationale for the use of acetylcholinesterase inhibitors in the therapy of Alzheimer̀s disease? Eur. J. Pharmacol. 346 (1998) 1−13.

[21] N.C. Inestrosa, A. Alvarez, C.A. Perez, R.D. Moreno, M. Vicente, C. Linker, O.I. Casanueva, C. Soto, Garrido, J. Acetylcholinesterase acceleratyes assembly of amyloid-beta-peptides into Alzheimer̀s fibrils: possible role of the peripheral site of the enzyme, Neuron 16 (1996) 881−91.

[22] A.E. Reyes, D.R. Perez, A. Alvarez, J. Garrido, M.K. Gentry, B.P. Doctor, N.C. Inestrosa, A monoclonal antibody against acetylcholinesterase inhibits the formation of amyloid fibrils induced by the enzyme, Biochem. Biophys. Res. Commun. 232 (1997) 652− 655.

[23] N.C. Inestrosa, A. Alvarez, J. Godoy, A. Reyes, G.V. De Ferrari, Acetylcholinesterase-amyloid-beta-peptide interaction and Wnt signaling involvement in Abeta neurotoxicitity, Acta Neurol. Scand. Suppl. 102 (2000) 53−56.

[24] D.J. Bonda, X. Wang, G. Perry, A. Nunomura, M. Tabaton, X. Zhu, M.A. Smith, Oxidative stress in Alzheimer disease: a possibility for prevention, Neuropharmacology 59 (2010) 290−294.

[25] J. Kumar, P. Meena, A. Singh, E. Jameel, M. Maqbool, M. Mobashir, A. Shandilya, M. Tiwari, N. Hoda, B. Jayaram, Synthesis and screening of triazolopyrimidine scaffold as multi-functional agents for Alzheimer's disease therapies, Eur. J. Med. Chem. 119 (2016) 260-277.

[26] M.L. Bolognesi, A. Cavalli, Multitarget Drug Discovery and Polypharmacology, ChemMedChem 11 (2016) 1190-92.

[27] S.O. Bachurin, E.V. Bovina, A.A. Ustyugov, Drugs in Clinical Trials for Alzheimer's Disease: The Major Trends, Med. Res. Rev. 37 (2017) 1186-1225.

[28] M.C. Carreiras, E. Mendes, M.J. Perry, A.P. Francisco, J. Marco-Contelles, The multifactorial nature of Alzheimer's disease for developing potential therapeutics, Curr. Top. Med. Chem. 13 (2013) 1745–1770.

[29] A.M. Hussin, F.A. Abu-Shanab, E.A. Ishak, Polycyclic pyridines: synthesis of pyridothienopyrimidines pyridothienotriazines and pyridothienotriazepines, Phosphorus Sulfur Silicon Relat. Elem. 159 (2000) 55-68.

[30] J. W itherington, V. Bordas, A. Gaiba, N.S. Garton, A. Naylor, A.D. Rawlings, B.P. Slingsby, D.G. Smith, A.K. Takle, R.W. Ward, 6-Aryl-pyrazolo[3,4-b]pyridines: potent inhibitors of glycogen synthase kinase-3 (GSK-3), Bioorg. Med. Chem. Lett. 13 (2003) 3055-3057.

[31] J. Witherington, V. Bordas, S.L. Garland, D.M.B. Hickey, R.J. Ife, J. Liddle, M. Saunders, D.G. Smith, R.W. Ward, 5-Aryl-pyrazolo[3,4-b]pyridines: potent inhibitors of glycogen synthase kinase-3 (GSK-3), Bioorg. Med. Chem. Lett. 13 (2003) 1577-1580.

[32] A. Straub, J.P. Stasch, C. Alonso-Alija, J. Benet-Buchholz, B. Ducke, A. Feurer, C. Fürstner, NO-independent stimulators of soluble guanylate cyclase, Bioorg. Med. Chem. Lett. 11 (2001) 781-784.

[33] A.K. Sharma, S. Chandra, Complexation of nitrogen and sulphur donor Schiff's base ligand to Cr(III) and Ni(II) metal ions: Synthesis, spectroscopic and antipathogenic studies, Spectrochim. Acta A 78 (2011) 337-342.

[34] R.N. Misra, D.B. Rawlins, H. Xiao, W. Shan, I. Bursuker, K.A. Kellar, J.G. Mulheron, J.S. Sack, J.S. Tokarski, S.D. Kimball, K.R. Webster, 1H-Pyrazolo [3,4-b]pyridine inhibitors of cyclin-dependent kinases, Bioorg. Med. Chem. Lett. 13 (2003) 1133-1136.

[35] R.N. Misra, H. Xiao, D.B. Rawlins, W. Shan, K.A. Kellar, J.G. Mulheron, J.S. Sack, J.S. Tokarski, S.D. Kimball, K.R. Webster, 1H-Pyrazolo[3,4-b]pyridine inhibitors of cyclin-dependent kinases: highly potent 2,6-difluorophenacyl analogues, Bioorg. Med. Chem. Lett. 13 (2003) 2405-2408.

[36] L. Meijer, M. Flajolet, P. Greengard, Pharmacological inhibitors of glycogen synthase kinase 3, Trends Pharm. Sci. 25 (2004) 471-480.

[37] H. De Mello, A.M. Echevarria, M. Bernardino, L. Canto-Cavalheiro, L. Leon, Antileishmanial pyrazolopyridine derivatives: synthesis and structure-activity relationship analysis, J. Med. Chem. 47 (2004) 5427-5432.

[38] M.S. Masoud, S.A. AbouEl-Enein, H.M. Kamel, Structural chemistry and thermal properties of some pyrimidine complexes, Indian J. Chem. 14 (2002) 297-303.

[39] S.M. Emam, F.A. El-Saied, S.A. AbouEl-Enein, H.A. El-Shater, Cobalt(II), nickel(II), copper(II), zinc(II) and hafnium(IV) complexes of N′-(furan-3-ylmethylene)-2-(4-methoxyphenylamino)acetohydrazide, Spectrochim. Acta A 72 (2009) 291-297.

[40] F.A. Attaby, A.H.H. Elghandour, A.M. Ali, Y.M. Ibrahim, Synthesis, characterization, and antiviral activities of pyridopyrazolotriazines, Phosphorus Sulfur Silicon Relat. Elem. 182 (2007) 133-149.

[41] F.A. Attaby, A.H.H. Elghandour, M.A. Ali, Y.M. Ibrahim, Synthesis, reactions, and antiviral activity of 1-(1H-Pyrazolo[3,4-b]pyridin-5-yl)ethanone and Pyrido[2′,3′:3,4]pyrazolo[5,1-c][1,2,4]triazine derivatives, Phosphorus Sulfur Silicon Relat. Elem. 181 (2006) 1087-1102.

[42] A.R. Azevedo, V.F. Ferreira, H. de Mello, L.R. Leao-Ferreira, A.V. Jabor, I.C.P.P. Frugulhetti, H.S. Pereira, N. Moussatche, A.M.R. Bernardino, Synthesis and biological evaluation of 1H-pyrazolo[3,4-b]pyridine-5-carboxylic acids against Vaccinia virus, Heterocycl. Commun. 8 (2002) 427-432.

[43] A. Hiremathad, R.S. Keri, A.R. Esteves, S.M. Cardoso, S. Chaves, M.A. Santos, Novel Tacrine-Hydrxyphenylbenzimidazole hybrids as potential multitarget drug candidates for Alzheimer's disease, EJMC 148 (2018) 255-267

[44] M. Jesus, O. Gasque, J. Marco-Contelles, Alzheimer's Disease, the "One-Molecule, One-Target" Paradigm, and the Multitarget Directed Ligand Approach, ACS Chem. Neurosci. 9 (2018) 401-403.

[45] M.A. Santos, K. Chand, S. Chaves, Recent progress in repositioning Alzheimer's disease drugs based on a multitarget strategy, Future Med. Chem. 8 (2016) 2113-2142.

[46] M. Marcade, J. Bourdin, N. Loiseau, H. Peillon, A. Rayer, D. Drouin, F. Schweighoffer, L. Desire, Etazolate, a neuroprotective drug linking GABA(A) receptor pharmacology to amyloid precursor protein processing, J. Neurochem. 106 (2008) 392-404.

[47] T. Umar, S. Shalini, M.K. Raza, S. Gusain, J. Kumar, W. Ahmed, M. Tiwari and N. Hoda, New amyloid beta-disaggregating agents: synthesis, pharmacological evaluation, crystal structure and molecular docking of N-(4-((7-chloroquinolin-4-yl)oxy)-3-ethoxybenzyl)amines, Medchemcomm. 9 (2018) 1891-1904.

[48] A. Salahuddin, A. Inam, R.L. van Zylb et al. Synthesis and evaluation of 7-chloro-4-(piperazin-1-yl)quinolinesulfonamide as hybrid antiprotozoal agents, Bioorg. Med. Chem. 21 (2013) 3080–3089.

[49] K.L. Sciarretta, D.J. Gordon, A.T. Petkova, R. Tycko, S.C. Meredith, Aβ40-Lactam(D23/K28) models a conformation highly favorable for nucleation of amyloid, Biochemistry 44 (2005) 6003–6014.

[50] J.L. Cummings, D.F. Benson, Subcortical dementia: Review of an emerging concept, Arch. Neurol. 41 (1984) 874-9.

[51] C. Lu, Y. Guo, J. Yan, Z. Luo, H.B. Luo, M. Yan, L. Huang, and X. Li, Design, Synthesis, and Evaluation of Multitarget-Directed Resveratrol Derivatives for the Treatment of Alzheimer's Disease, J. Med. Chem. 56 (2013) 5843-5859.

[52] B. Ou, M. Hampsch-Woodill, R.L. Prior, Development and validation of an improved oxygen radical absorbance capacity assay using fluorescein as the fluorescent probe, J. Agric. Food Chem. 52 (2004) 48-54.

[53] G. Lavecchia, S. Berteina-Raboin, G. Guillaumet, Synthesis and functionalisation of 1H-pyrazolo[3,4-b]pyridines involving copper and palladium-promoted coupling reactions, Tetrahrdron letters, 45 (2004) 2389-2392.

[54] A. Salahuddin, A. Inam. R.L. van Zyl, D.C. Heslop, C.T. Chen, F. Avecilla, S.M. Agarwal, A. Azam, Synthesis and evaluation of 7-chloro-4-(piperazin-1-yl)quinoline-sulfonamide as hybrid antiprotozoal agents, Bio. Med. Chem, 21 (2013) 3080-3089.

[55] B. Brus, U. Kosak, S. Turk, A. Pislar, N. Coquelle, J. Kos, J. Stojan, J. P. Colletier, S. Gobec, Discovery, biological evaluation, and crystal structure of a novel nanomolar selective butyrylcholinesterase inhibitor, J. Med. Chem. 57 (2014) 8167-8179.

[56] J. Fuhrmann, A. Rurainski, H. P. Lenhof, D. Neumann, A new Lamarckian genetic algorithm for flexible ligand-receptor docking, J. Comput. Chem. 31 (2010) 1911–1918.

[57] A. Gupta, A. Gandhimathi, P. Sharma, B. Jayaram, ParDOCK: An All Atom Energy Based Monte Carlo Docking Protocol for Protein-Ligand Complexes, Protein Pept. Lett. 14 (2007) 632-646.

[58] T. Jain, B. Jayaram, An all atom energy based computational protocol for predicting binding affinities of protein-ligand complexes, FEBS Lett. 579 (2005) 6659-6666.

[59] T. Singh, D. Biswas, B. Jayaram, AADS-an automated active site identification, docking, and scoring protocol for protein targets based on physicochemical descriptors, J. Chem. Inf. Model. 51 (2011) 2515-2527.

[60] W.L. DeLano, PyMOL Reference Manual, DeLano Scientific LLC, San Carlos, CA, USA, 2003.

[61] N. Walker, D. Stuart, An empirical method for correcting diffractometer data for absorption effects, Acta Crystallogr., Sect. A: Found. Crystallogr. 39 (1983) 158−166.

[62] G.M. Sheldrick, Crystal structure refinement with SHELXL, Acta Crystallogr., Sect. C: Struct. Chem. 71 (2015) 3−8.

[63] L.J. Farrugia, WinGX and ORTEP for Windows: an update, J. Appl. Crystallogr. 45 (2012) 849−854.

[64] G.L. Ellman, K.D. Courtney, V. Andres jr., R.M. Featherstone, A new and rapid colorimetric determination of acetylcholinesterase activity, Biochem. Pharmacol. 7 (1961) 88-95.

[65] A. Manral, V. Saini, P. Meena, M. Tiwari, Multifunctional novel diallyl disulfide (DADS) derivatives with β-amyloid-reducing, cholinergic, antioxidant and metal chelating properties for the treatment of Alzheimer's disease, Bioorg. Med. Chem. 23 (2015) 6389-403.

[66] B.P. Repsold, S.F. Malan, J. Joubert, D.W. Oliver, Multi-targeted directed ligands for Alzheimer's disease: design of novel lead coumarin conjugates, SAR QSAR Environ. Res. 29 (2018) 231-55.

- 2-(piperazin-1-yl)-N-(1H-pyrazolo[3,4-b]pyridin-3-yl)acetamides are described as a new class of selective and potent acetylcholinesterase (AChE) inhibitors
- Multifunctional anti-Alzheimer's agents with acetylcholinesterase and butyrylcholinesterase inhibition, Aβ aggregation inhibition, Aβ disaggregation, antioxidation and metal-chelation properties.
- The most potent molecule amongst the derivatives exhibited excellent anti-AChE activity with IC50 = 4.8 nM.
- *In vitro* study revealed that all the compounds are capable of inhibiting self-induced β-amyloid aggregation with the highest inhibition percentage to be 81.65%.
- $A\beta_{1-42}$ aggregation was ascertained by TEM analysis.